Title

Mechanisms of Force Generation by Actin Filament Associated Proteins in Budding Yeast Clathrin-mediated Endocytosis

Author

Hill, Jennifer M

Publication Date

2024

Peer reviewed|Thesis/dissertation

Mechanisms of Force Generation by Actin Filament Associated Proteins in Budding Yeast Clathrin-mediated Endocytosis

By

Jennifer Hill

A dissertation submitted in partial satisfaction of

the requirements for the degree of

Doctor of Philosophy

in

Molecular and Cell Biology

in the

Graduate Division

of the

University of California, Berkeley

Committee in charge:

Professor David G. Drubin, Chair
Professor Matthew D. Welch
Professor Ahmet Yildiz
Professor Daniel A. Fletcher

Spring 2024

Mechanisms of Force Generation by Actin Filament Associated Proteins in Budding Yeast Clathrin-mediated Endocytosis

By
Jennifer Hill

Abstract

Mechanisms of Force Generation by Actin Filament Associated Proteins in Budding Yeast Clathrin-mediated Endocytosis

by

Jennifer Hill

Doctor of Philosophy in Molecular and Cell Biology

University of California, Berkeley

Professor David G. Drubin, Chair

The high turgor pressure across the plasma membrane of yeasts creates a requirement for substantial forces, produced by polymerization of an actin filament network, for clathrin-mediated endocytosis (CME). Endocytic internalization is impeded in the absence of fimbrin, an actin filament crosslinking protein called Sac6 in budding yeast. In the first chapter of this dissertation, I use live-cell microscopy to gain new insights into the role of actin filament crosslinking proteins in force generation. Quantitative measurement of the numbers of fimbrin and transgelin molecules at sites of CME reveals an interplay between recruitment of these two actin crosslinking proteins. Manipulation of turgor pressure shows that sites with more fimbrin are more effective at internalization under high load. Super-resolved microscopy of actin patches in fixed yeast reveals that sites with more fimbrin also have a higher density of actin filaments, implicating crosslinking proteins in assisting in force generation by the actin network during CME under increased load.

In Chapter 2, I use simulations of an experimentally constrained, agent-based mathematical model of CME to recapitulate the result that endocytic networks with more double-bound fimbrin internalize the plasma membrane against elevated turgor pressure more effectively. Networks with large numbers of crosslinks also have more growing actin filament barbed ends at the plasma membrane, where the addition of new actin monomers contributes to force generation and vesicle internalization. These results provide a richer understanding of the crucial role played by actin filament crosslinking proteins during actin network force generation, highlighting the contribution of these proteins to the self-organization and force generation of the actin filament network.

The myosin-Is, Myo3 and Myo5 in budding yeast, are also implicated in force generation and assist in assembly of the actin network during CME. The myosin-Is consist of a motor domain, a membrane binding tail homology 1 (TH1) domain, and an Src

homology 3 (SH3) domain that works in concert with a central acidic (CA) region to activate the Arp2/3 complex and promote branched actin assembly. In the third chapter of this dissertation, I examine the ability of Myo5 domain mutant proteins to complement each other in diploid budding yeast. Through a growth assay and live cell microscopy, I reveal that the force generating motor domain and NPF activity from the SH3 domain of Myo5 each must be coupled to the membrane binding TH1 domain for successful progression of CME. However, motor and NPF activity are modular and separable, providing interesting insight into the function of the essential myosin-I in actin network assembly and force generation during budding yeast CME.

For my family and friends, who each inspire me in their own ways

Table of Contents

List of figures and tables

Acknowledgements

First and foremost, I would like to thank David and Georjana, who work tirelessly to create a lab environment that is intellectually stimulating, values learning, and fosters scientific curiosity. David's mentorship has made me into the independent scientist I am today and has thoroughly prepared me to enter the next stage of my career and beyond. A PhD is a hugely formative stage in any scientist's career, and I could not be more happy to have received my training in the Drubin/Barnes lab.

I also could not have succeeded in this PhD without the help of my various mentors in the lab: Ross, Jonathan, Yidi, and Zane. I was always made to feel like there were no stupid questions with them, and absolutely took advantage of that to ask all the stupid questions in the world. A training environment like that is truly hard to come by and I am so grateful to them for their guidance throughout this process. Their knowledge and expertise were indispensable and advice was freely given. I thank them for the time they dedicated to my PhD throughout the years.

To Julia, Sam, Yui, Paul, and all of the friends I made in the Drubin lab, thank you for being my motivation to go to work on the days where the fifth repeat of the same PCR wasn't motivation enough. Not only are you all incredibly talented scientists, you are amazing friends and so much fun to be around. I'll always look back on the hours spent doing the crossword, playing Geoguessr, and our infamous poker nights with so much fondness and nostalgia. Let's keep being awesome scientists and amazing people in all of our future endeavors, and I can't wait to see where we all end up.

To my best friends, Sophie and Siena, thank you for your absolutely endless love and support while I pursued this six-year project of putting a Dr. in front of my name. I truly can't imagine how I would have gotten this far without all of your advice when I asked for it, and your patience to just listen to me rant when I needed it. You both have become my family here and are the number one thing making it difficult to search for jobs anywhere outside of the Bay Area (which I totally don't mind by the way). I'm so lucky to have made such amazing friends who I know I'll have with me for the rest of my life.

Finally, thank you to my family who have been supporting me for 27 years now. My parents have always been my inspiration to succeed in my education and probably the first reason I considered pursuing a PhD at all. Being raised in a family full of physicists and computer scientists was occasionally tiresome, but also such an important factor in the development of my own scientific curiosity and drive. I still remember the day you suggested scientific research as a career path, and all the doors you've opened along the way to help me get here have been so integral to my success. Thank you for raising me to be the smart, independent, and curious person I am, I could not have done this without you.

Chapter 1: Introduction

Clathrin-mediated endocytosis (CME) is the process by which cells take up membrane-bound and soluble molecules from their surface and environment through the internalization of a clathrin-coated vesicle. CME is highly conserved from budding yeast to mammalian cells, as it is a major pathway for internalizing necessary cellular building blocks and down-regulating signal transduction by membrane receptors. The process can be described as consisting of a set of modules, each composed of proteins that work in concert to recruit cargo, adaptors, and coat proteins, build an actin filament network to invaginate the membrane against resistive membrane forces, and release the nascent vesicle into the cytoplasm (Goode et al., 2015; Kaksonen et al., 2005). The budding yeast *Saccharomyces cerevisiae* is an ideal organism for studying CME because the proteins in each of these modules and their biochemical properties are well-characterized and they show a high level of conservation to mammalian CME proteins (Boettner et al., 2011).

The timing and recruitment of the majority of CME proteins is well established, and the proteins have been assigned to unique modules, each with its own role in the process (Kaksonen et al., 2005). The process begins when a set of early module proteins including clathrin and the Eps15 homology domain protein Ede1 arrive at the membrane and recruit cargo to be internalized (Kaksonen et al., 2005; Newpher et al., 2005; Stimpson et al., 2009). In budding yeast, the membrane is under high tension compared to many other cell types. Therefore, internalization requires force production by polymerization of a branched actin network and actin associated proteins such as crosslinkers and myosins (Fig. 1.1) (Kaksonen et al., 2005; Moseley & Goode, 2006; Sun et al., 2006). Formation of this actin network is nucleated by proteins in the WASP/myosin module, and the myosin-I likely also contributes to force generation through its motor activity (Pedersen et al., 2023; Sun et al., 2006). Once the membrane is fully invaginated, scission factors arrive at the omega-shaped pit to pinch off the membrane, and a fully formed vesicle is released (Kaksonen et al., 2005; Liu et al., 2009).

While actin filament assembly is associated with CME from yeast to humans (Kaksonen et al., 2003; Merrifield et al., 2002), the high turgor pressure in yeast creates a particularly pronounced requirement for forces generated by polymerization of a branched actin network and myosin motor activity (Aghamohammadzadeh & Ayscough, 2009; Pedersen et al., 2023; Sun et al., 2006). The Arp2/3 complex nucleates a branched actin filament network when activated by the yeast WASP, also known as Las17, and the CA domain of type-I myosins (Mund et al., 2018; Sun et al., 2006). Adaptor proteins Sla2 and Ent1/2 couple the actin filament network to the growing membrane invagination (Skruzny et al., 2012) (Fig. 1.1). Additional actin-associated proteins such as myosins (Pedersen & Drubin, 2019; Sun et al., 2006), capping proteins (K. Kim et al., 2004), the actin-filament severing protein cofilin (Okreglak & Drubin, 2007), and actin crosslinking proteins (Goode et al., 2015; Picco et al., 2018) all play important roles in the process, but how these

proteins work together to build an actin network capable of sufficient force production to drive membrane bending is still not fully understood.

Crosslinking proteins are important actin associated proteins involved in a wide variety of cellular processes, from cell migration to mechanosensing (Krey et al., 2016; Krey & Barr-Gillespie, 2019; Mellor, 2010; Mogilner & Rubinstein, 2005). While there are many classes of actin filament crosslinking proteins, all use actin binding domains to form crosslinks between actin filaments, which can lead to regulation of actin assembly and disassembly, assist in actin-based cellular movement, and organize filaments into parallel or antiparallel bundles (Lappalainen, 2016; Pollard, 2016; Pollard et al., 2000; Rajan et al., 2023). The crosslinkers involved in budding yeast endocytosis are fimbrin, also known as plastin in animals, and transgelin. Fimbrin is a monomeric protein with two actin-binding domains (ABD's), each consisting of two calponin homology (CH) domains, which make up the core protein and confer actin binding activity, along with a Ca^{2+} regulatory domain (Hanein et al., 1998). Fimbrin is capable of bundling actin filaments into both parallel and antiparallel structures (Mei et al., 2022; Skau et al., 2011), and this diversity of function leads to its presence in a wide range of cellular structures, including microvilli and the contractile ring (Bretscher & Weber, 1980; Laporte et al., 2012). Transgelin is a small, 22-kD monomeric protein containing only a single CH domain (Li et al., 2008). The mechanism behind transgelin binding to and crosslinking actin filaments is still controversial, but it has been shown to induce formation of tight parallel actin bundles *in vitro* (Winder et al., 2003). Actin filament bundling by crosslinkers has the ability to alter the viscoelastic properties of the resulting actin network (Planade et al., 2019; Reda et al., 2022), but the exact impact of actin filament crosslinking on the function of the resulting actin filament networks remains unclear.

In addition to generating forces through assembly against membranes, actin networks are capable of generating forces through the activity of myosins. The myosin family members are the only known actin-associated motor proteins involved in a wide range of force-generating and force-sensing cellular processes (Hartman & Spudich, 2012). The class of myosins involved in CME is the type I myosins, or myosin-Is (McIntosh & Ostap, 2016). Myosin-Is differ from the conventional myosin-II motor involved in muscle contractility in that they are monomeric, non-processive motors, capable of binding both actin filaments through a motor domain, and membranes through a tail domain (S. V. Kim & Flavell, 2008; McConnell & Tyska, 2010). This membrane binding activity implicates myosin-Is in a multitude of membrane-associated force production processes such as filopodial extrusion and formation of invadosomes (Ouderkirk & Krendel, 2014; Ruppert et al., 1995), and makes them the ideal protein to act in CME as a connection between the endocytic membrane and the polymerizing actin network (Fig. 1.1) (Pedersen & Drubin, 2019). The budding yeast myosin-Is are long-tailed myosins with an actin binding motor domain, membrane binding tail homology (TH) domain, and Arp2/3 complex activating Src homology 3 (SH3) and central acidic (CA) domains (Lewellyn et al., 2015; Pedersen &

Drubin, 2019). While the function and properties of these modular myosin-I domains have been well-characterized, the interplay and dependencies between the individual domains have not been studied.

The dynamics and functions of actin associated proteins in CME have been studied for decades using a wide array of techniques including biochemical assays, live cell microscopy, cryo-electron microscopy, and genetic screens. However, the small size of the CME-associated actin network has made it difficult to determine the effect of individual actin-associated proteins on the structure and dynamics of the actin network as a whole. In recent years, mathematical models of the actin network have been developed to begin to expand our understanding of this topic (Akamatsu et al., 2020; Dmitrieff & Nédélec, 2015; Mund et al., 2018; Nickaeen et al., 2019; Wu et al., 2021). These models span a wide range of scales from extremely fine-grain molecular dynamics simulations of the crosslinking protein fascin bundling actin filaments (Wu et al., 2021), to medium-grain models based on the physical theory of membrane mechanics (Dmitrieff & Nédélec, 2015), to more coarse-grain agent-based simulations of the entire actin network (Akamatsu et al., 2020; Mund et al., 2018). Each type of mathematical model has its advantages and disadvantages, wherein models that more closely resemble the reality of the biological system incur considerable computational costs (Pleyer & Fleck, 2023). Therefore, assumptions and simplifications must be made in any mathematical model of a biological system in order to answer questions and formulate hypotheses with any efficiency (Pleyer & Fleck, 2023). Agent-based models have the advantage of stochastically modeling each agent and its interactions with other agents in the system, capturing heterogeneity and spatial information, but they can be computationally costly if a large number of agents or properties are included in the model (Pleyer & Fleck, 2023). For this reason, only the proteins of interest to a particular biological question are included in these models, and assumptions are made to reduce the number of properties being modeled for each agent in the system (Pleyer & Fleck, 2023). Agent-based models of CME have been used to show the importance of the precise localization of the Arp2/3 complex in seeding an actin network for internalization of a vesicle (Mund et al., 2018), and to explore adaptive mechanisms for the actin network during endocytosis under various physical environments (Akamatsu et al., 2020).

A major strength of agent-based mathematical modeling is the ability to combine it with experimental data, generating a feedback loop between the hypotheses generated by the model and experimental results that either confirm those hypotheses or motivate alterations to the model. In this dissertation, I present a series of experiments and simulations that provide insight into the roles of two classes of actin filament-associated proteins: crosslinking proteins and myosins. Using live cell microscopy, I show that the relative abundance of crosslinkers is essential for the cell's response to conditions of high turgor pressure. Using mathematical modeling, I identify a role for actin filament crosslinking proteins in organizing growing actin filaments to optimize force production by

the actin network. Finally, I use live cell microscopy to identify a modular interaction between the membrane binding domain of myosin-I and the motor and Arp2/3 complex-activating SH3 domains of the same protein. I propose that the introduction of myosin-I motor and NPF activity to the mathematical model is an appropriate modification that would more accurately capture the formation of a force-generating branched actin network during CME.

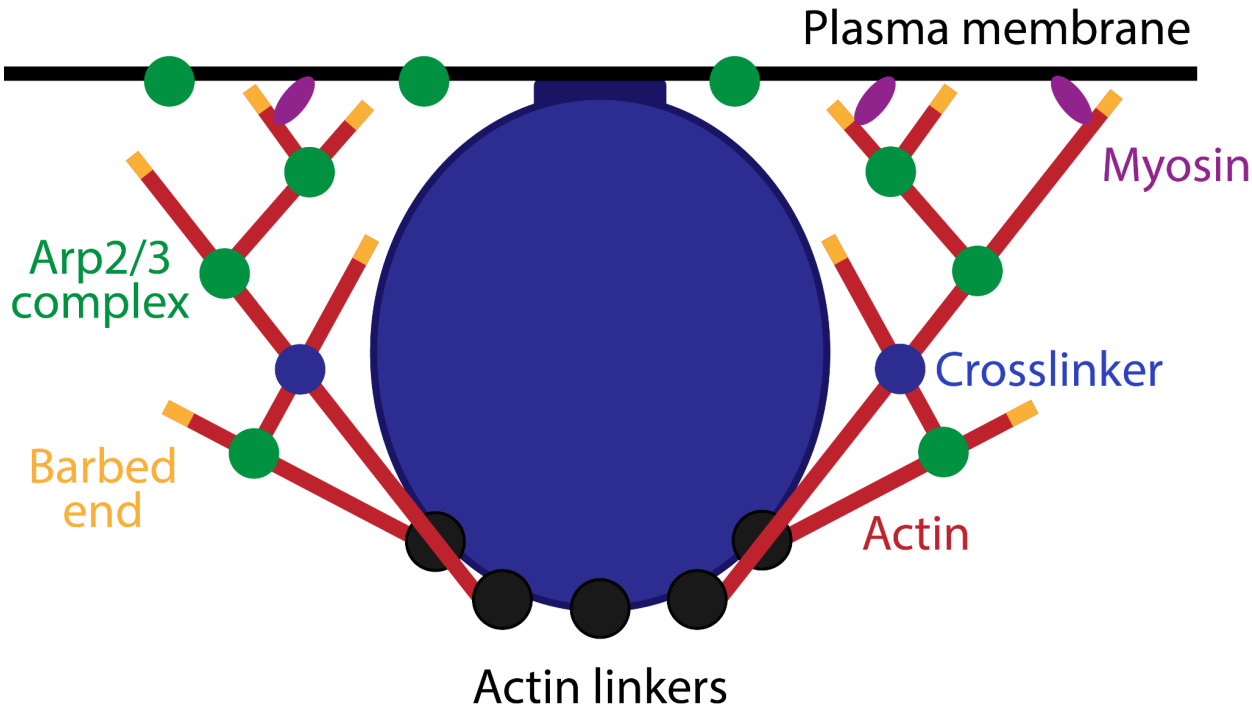

Figure 1.1: Schematic representation of CME in budding yeast. The flat plasma membrane is represented by a black line with an invagination represented in blue on the cytoplasmic side. Actin linkers (black) are bound to the membrane and clathrin at the tip of the vesicle and actin filaments that grow towards the membrane are shown in red, with barbed ends in yellow. The Arp2/3 complex (green) is localized to the membrane where it binds actin filaments and nucleates a daughter actin filament to form a branched actin network. Crosslinkers (blue) bind and bridge two actin filaments and myosins (purple) bind the flat plasma membrane and act as an anchor for actin assembly.

Chapter 2: Actin filament crosslinking proteins contribute to force generation by the actin network under conditions of high turgor pressure

2.1: Introduction

At least two actin crosslinking proteins are involved in CME in budding yeast. The yeast fimbrin, Sac6, and the yeast transgelin, Scp1, crosslink actin filaments *in vitro*, and are localized to the actin filament network at endocytic sites (Goodman et al., 2003; Winder et al., 2003). While fimbrin and transgelin undergo genetic dosage compensation (Gheorghe et al., 2008), the effect of their relative expression levels on their recruitment to and function at endocytic sites has not been reported. Yeast fimbrin is essential for CME (Kaksonen et al., 2005), and its absence leads to a growth defect (Goodman et al., 2003). Additionally, actin networks assembled *in vitro* from yeast extracts lacking fimbrin have a lower elastic modulus than networks assembled in wild-type yeast extracts, indicating that fimbrin contributes to the stiffness of actin networks *in vitro* (Planade et al., 2019; Reda et al., 2022). The absence of transgelin exacerbates the endocytic defects observed in cells lacking fimbrin, but the absence of transgelin alone has only a minor effect on cell growth and endocytosis (Goodman et al., 2003) or the elastic modulus of actin filament networks assembled in yeast extracts (Planade et al., 2019). For these reasons, transgelin is a relatively under-studied component of budding yeast CME machinery.

In this chapter, we investigated the effect of actin filament crosslinking protein abundance on clathrin-mediated endocytosis in budding yeast. We used quantitative microscopy to determine the numbers of yeast fimbrin and yeast transgelin molecules at CME sites in cells grown under various conditions and tested for an association between the number of crosslinking proteins and endocytic success at high turgor pressure. Markedly more fimbrin is present at CME sites than transgelin, and additional fimbrin can assist in internalization during the adaptive response to hypotonic shock. We use super-resolution microscopy to assess the impact of actin filament crosslinking on the size and density of actin networks in fixed cells. These studies identified a novel role for actin filament crosslinking proteins in modulation of actin network force generation during budding yeast CME.

2.2: Results and discussion

2.2.1: Interplay between fimbrin and transgelin actin filament crosslinking protein recruitment to CME sites

The maximum number of molecules of the most abundant actin filament crosslinking protein at CME sites, fimbrin, has previously been estimated using quantitative

fluorescence microscopy (Sun et al., 2019). We used the same quantitative microscopy method to measure the maximum number of transgelin molecules arriving at endocytic sites. Transgelin is a less abundant actin filament crosslinking protein. We used the ratio between the maximum fluorescence intensities of endogenously labeled Las17-GFP, a protein whose abundance at endocytic sites has been measured (Sun et al., 2019), and GFP-tagged transgelin in the same field of view to determine that the maximum number of transgelin molecules recruited to CME sites is 40±15 (Fig. 2.2A, 2.2B).

Transgelin protein levels have been reported to increase upon deletion of the gene encoding yeast fimbrin, *SAC6* (Gheorghe et al., 2008). We tested how fimbrin absence affects the number of transgelin molecules at CME sites and found that more transgelin molecules are recruited to CME sites in cells lacking fimbrin (58±40, $p<0.0005$) relative to CME sites in wild-type cells (Fig. 2.1A, 2.1B). This observation suggests that dosage compensation by transgelin for fimbrin absence contributes to increased transgelin recruitment to CME sites. We also found that transgelin lifetime at CME sites increases in the absence of fimbrin, consistent with previously published results showing that absence of fimbrin leads to increased actin patch lifetimes (Gheorghe et al., 2008; Kaksonen et al., 2005)) (Fig. 2.2C).

Next, we investigated whether previously reported increased fimbrin expression when transgelin is absent similarly increases fimbrin recruitment to CME sites. In wild-type cells, the maximum number of fimbrin molecules at CME sites was previously determined to be 545±135 (Sun et al., 2019). Using the fluorescence intensity of GFP-tagged fimbrin in wild-type cells as the standard, the number of fimbrin molecules recruited to endocytic sites in cells lacking transgelin was slightly higher than in wild-type cells, although the difference was not statistically significant (574±205 $p=0.3087$). Thus, in the absence of transgelin, changes in fimbrin recruitment to CME sites were at best small (Fig. 2.1C and Fig. 2.1D). Additionally, transgelin absence did not significantly increase the fimbrin lifetime at CME sites, consistent with a previously reported modest endocytic defect observed in cells lacking transgelin (Goodman et al., 2003) (Fig. 2.2D). These results indicate that the reduced requirement for transgelin in crosslinking actin filaments at CME sites relative to fimbrin might be at least partially explained by its relatively low abundance at CME sites compared to the fimbrin.

2.2.2: Actin filament crosslinking protein importance for CME internalization tested under high turgor pressure *in vivo*

We next investigated the effect of varying numbers of crosslinking proteins on the efficiency of CME *in vivo*. In the following experiments, we deleted the gene encoding transgelin to eliminate the complication of differing contributions from multiple types of crosslinking proteins. We used hypotonic shock to increase turgor pressure to the point when about half of the CME events failed (Riggi et al., 2018, 2019), and compared numbers of fimbrin molecules at sites that successfully internalize or fail to internalize. We also

deleted the gene encoding the glycerol export protein, Fps1, which is important to restore membrane tension in response to hypotonic shock, extending the time during which cells have increased turgor pressure (Riggi et al., 2018; Tamás et al., 1999). Before shock, the fraction of endocytic sites that internalize in wild-type cells, using the endocytic coat protein Sla1 as a marker for internalization, is 0.89±0.07, while after hypotonic shock, the fraction of sites that internalize is 0.53±0.14 (Fig. 2.4A and Fig. 2.4B). The lifetimes of Sla1 and the actin-binding protein Abp1 at CME sites also increase upon hypotonic shock, indicative of a defect in CME (Fig. 2.4C and Fig. 2.4D).

We then generated strains with varying copy numbers of the fimbrin gene, *SAC6*: a heterozygous diploid (*SAC6/sac6Δ*), a wild-type diploid (*SAC6/SAC6*), a wild-type haploid (*SAC6*), and a haploid bearing a duplication of the gene encoding fimbrin at the endogenous locus (*SAC6* dupl.). We used quantitative microscopy to measure the maximum number of fimbrin molecules arriving at endocytic sites after hypotonic shock in these strains and found a range of numbers of fimbrin molecules at each site (Fig. 2.3A, Fig. 2.3C, and Fig. 2.4E). We also quantified the fraction of endocytic sites that internalize in each of these strains after hypotonic shock and found that strains with an increased copy number of the gene encoding fimbrin have a higher fraction of sites that internalize compared to strains with a lower gene dosage (Fig. 2.3B, Fig. 2.3C, and Fig. 2.4F). Taken together, these data indicate that increased numbers of crosslinking proteins contribute to internalization under conditions of high turgor pressure and suggest that crosslinking proteins may be involved in an adaptive response to provide additional force for internalization.

To investigate the relationship between crosslinking proteins and CME efficiency at individual CME sites, we categorized endocytic events as internalized or failed based on the movement of both fimbrin and Abp1 away from the membrane and quantified the maximum number of fimbrin molecules recruited to these sites (Fig. 2.5A). Sites that internalize have significantly more crosslinking proteins than sites that fail to internalize (Fig. 2.5B). The same result was observed using Sla1, associated with the vesicle coat rather than an actin network component, as a marker for endocytic internalization (data not shown). Additionally, we also observed that sites that successfully internalize have significantly higher Abp1 fluorescence intensity, likely reflecting more assembled actin, than sites that fail to internalize (Fig. 2.5C). However, the ratio of the number of fimbrin molecules to Abp1 fluorescence intensity is higher for sites that internalize, indicating that these actin filaments are more saturated with crosslinking proteins than actin filaments at sites that fail to internalize (Fig. 2.5D). Taken together, these data demonstrate that CME sites that recruit more crosslinking proteins are better able to internalize and show that the importance of actin filament crosslinking proteins for successful CME internalization is increased under conditions of high turgor pressure.

2.2.3: Super-resolution microscopy of actin patches in fixed yeast reveals interplay between actin crosslinking and network size

In order to investigate the interplay between actin filament crosslinking and the size of resulting actin patches, we used super-resolution microscopy to visualize actin patches in fixed budding yeast cells. We stained fixed yeast for actin filaments with phalloidin-AF647 and used stochastic optical reconstruction microscopy (STORM) to image actin patches with the focal plane at the bottom of the cell. Additionally, we took conventional microscopy images of GFP-tagged Sac6 to determine the relative crosslinking protein abundance at each site, and mScarlet-tagged Rvs167 as a marker for late stage endocytic events to ensure that all analyzed patches were in the same stage of endocytosis.

STORM imaging of phalloidin-AF647 revealed actin patches at the bottom plane of the cell, and actin cables were also visible in most cells (Fig. 2.6A). Individual actin patches were then segmented from the image, and Sac6-GFP and Rvs167-mScarlet signal were overlaid with the STORM image (Fig. 2.6B). Patches were manually picked based on the quality of signal in all three channels, and radii in X and Y were determined using the full width half maximum (FWHM) of phalloidin signal in the STORM image (Fig. 2.6C). Interestingly, plotting the area of the actin patches from STORM images against the relative intensity of Sac6 signal at the same patch revealed no correlation between actin patch size and abundance of actin crosslinking proteins (Fig. 2.6D).

In order to exaggerate effect size, we compared the area of the actin patches from wild-type cells to those from *SAC6* dupl. cells, which recruit approximately twice as many molecules of Sac6 to endocytic sites, on average (Fig. 2.4E). While the increase in actin patch size in *SAC6* dupl. cells from wild-type is not statistically significant, we did observe a wider variation in patch sizes in these cells (Fig. 2.6E). Additionally, patches in *SAC6* dupl. cells have significantly higher overall intensity and density of phalloidin signal (Fig. 2.6F and Fig. 2.6G). This suggests that while the increased abundance of actin crosslinking proteins in an actin network does not necessarily affect its size, it does coincide with patches with a higher density of actin filaments, and more actin overall.

2.2.4: Conclusions

In this chapter, we set out to determine the effect of actin filament crosslinking protein abundance in force generation during CME in budding yeast. We quantified the maximum number of molecules of fimbrin and transgelin arriving at CME sites and found that there are around ten times more fimbrin molecules than transgelin molecules on average. We found that deletion of the gene encoding fimbrin leads to compensatory recruitment of transgelin to sites of endocytosis. To count fimbrin and transgelin molecules, we used a quantitative microscopy technique that allowed us to compare numbers of crosslinking proteins at individual CME sites in various genetic backgrounds. Wild-type yeast recruit about 545 molecules of fimbrin and 40 molecules of transgelin for a total of about 595 crosslinking proteins per CME site.

Additionally, we showed that in live cells, CME sites with more crosslinking proteins are more likely to internalize against increased resistive forces, implicating crosslinking proteins as factors capable of assisting in force generation by the actin network. The actin networks at sites that internalize against high resistive forces are also more saturated with crosslinking proteins than sites that do not internalize, hinting at a ratiometric effect of concentrating crosslinking proteins in the actin network. Super-resolution microscopy of actin patches in fixed yeast reveals that increasing the abundance of actin crosslinking proteins at CME sites leads to more dense packing of actin filaments in the actin network. Taken together, the data in this chapter shed light on the role of crosslinking proteins in the actin network at CME sites in assisting in force generation, especially under conditions of high resistive forces.

2.3: Methods

Yeast strains

All budding yeast strains were grown in standard rich media (YPD) at 25°C since *sac6Δ* strains are temperature sensitive. The strains used in this study were derived from the wild-type diploid strain DDY1102 using standard techniques and are listed in Table 2.1. *SAC6* and *SAC6-GFP* duplication strains were generated following the technique described previously (Huber et al., 2014). Deletion of *SCP1* was constructed as described previously (Longtine et al., 1998). The resulting strains were verified by DNA sequencing.

Live-cell imaging

Cells were grown to mid-log phase in imaging media (synthetic minimal media supplemented with adenine, l-histidine, l-leucine, l-lysine, l-methionine, uracil, and 2% glucose) at 25°C and adhered to coverslips coated with 0.2 mg/ml concanavalin A. For quantitative microscopy experiments, reference cells were also grown to mid-log phase in imaging media at 25°C, incubated with FM4-64 (10 μg/mL, Molecular Probes), and adhered to the same coverslips as the reference strain. For hypotonic shock experiments, cells were grown to mid-log phase in imaging media containing 1M sorbitol at 25°C, adhered to coverslips with 0.2 mg/ml concanavalin A, then washed once into imaging media containing 0.25M sorbitol five min before imaging.

Quantitative fluorescence microscopy was performed using a Nikon Ti2-E inverted microscope with an Oko Labs environmental chamber pre-warmed to 25°C. GFP and FM4-64 were excited by a 488-nm laser and mRFP was excited by a 561-nm laser using highly inclined and laminated optical sheet (HILO) microscopy to illuminate the medial focal plane of the sample using a LUNF 4-line laser launch (Nikon Instruments, Melville, NY) and an iLas2 TIRF/FRAP module (Gataca Systems, Massy, France). A FITC emission filter was used to filter GFP and a Cy3 emission filter was used to filter RFP and FM4-64. Movies

were acquired using the Nikon NIS Elements software with a Nikon 60X CFI Apo TIRF objective (NA 1.49) and an Orca Fusion Gen III sCMOS camera (Hamamatsu, Hamamatsu City, Japan) at 1 X magnification. A single FM4-64 image was acquired using a 500 ms exposure time and single-channel and dual-channel movies were collected by acquiring images with 500 ms exposure times for 1 min.

Microscopy of Sla1-GFP and Abp1-mRFP was performed using a Zeiss LSM900 with Airyscan 2.0 detection and a stage pre-warmed to 25°C. Two color images of the medial focal plane were acquired using a Zeiss 60X objective (NA 1.4) by Zen Blue software in frame sequential acquisition mode, 5.0x zoom, and maximum laser scan speed at 1.7 fps. GFP and RFP were imaged with 3% laser power, 850V gain, and 1.0 digital gain. Laser lines were 488 nm for GFP and 561 nm for RFP. Post-acquisition, images were processed in Zen Blue with standard airyscan processing using auto filtering.

Image Analysis

All image analysis was performed using Fiji software (National Institutes of Health). All movies were subjected to background subtraction and photobleaching correction (Kaksonen et al., 2003). A median filter was used to quantify GFP-tagged fimbrin and transgelin molecule numbers to subtract cytosolic background from patches, as described previously (Picco & Kaksonen, 2017). 2D particle tracking software from the MosaicSuite (Sbalzarini & Koumoutsakos, 2005) was used to track fimbrin, transgelin, and Abp1 protein dynamics and trajectories were selected by visual inspection. Trajectories with lifetimes of less than two seconds, or that could not be clearly resolved from another patch, were excluded from our analysis. Maximum fluorescence intensities and fimbrin and transgelin patch lifetimes were extracted from the trajectories using custom code in Python (3.7) with Jupyter Notebook (Project Jupyter). This code is available at the following website: https://github.com/DrubinBarnes/YeastTrackAnalysis. The ratio between fluorescence intensities in the reference and query cells was used to determine molecule numbers as described previously (Sun et al., 2019).

For quantification of patch internalization and Sla1-GFP and Abp1-mRFP lifetimes, radial kymographs were generated from cells and chosen at random to be measured. For Airyscan movies, the patch was judged as "internalized" if it moved at least 200 nm toward the cell interior. The patch was judged as "failed" if it did not move toward the cell interior, moved fewer than 200 nm toward the cell interior, or moved toward the cell interior before returning to its original position.

3D-STORM

Cells were adhered to coverslips as described for live cell imaging experiments, and 16% paraformaldehyde (Electron Microscopy Sciences) was added directly to the coverslip to a final concentration of 4% followed by a 15 minute incubation. Samples were then

quenched with 50 mM NH_4Cl in CS (cytoskeleton) buffer (10mM MES buffer, 150 mM NaCl, 5mM EGTA, 5 mM glucose, 5 mM $MgCl_2$, pH 6.1) for five minutes with gentle shaking, twice. Samples were then permeabilized in CS buffer containing 5% w/v bovine serum albumin (BSA) and 0.5% Triton X-100 for 30 minutes with gentle shaking. Phalloidin AF-647 was added to the samples to a final concentration of 0.5 μM and incubated for two hours with gentle shaking.

Samples were washed into a standard STORM imaging buffer containing 5% (wt/vol) glucose, 100 mM cysteamine, 0.8 mg/ml glucose oxidase, and 40 μg/ml catalase in 1 M Tris-HCl (pH 7.5) (Huang et al., 2008; Rust et al., 2006). Imaging was performed on a homebuilt setup (Wojcik et al., 2015), with a modified Nikon Eclipse Ti-U inverted fluorescence microscope and a Nikon CFI Plan Apo λ 100× oil immersion objective (NA 1.45). Dye molecules were photo switched and imaged in the dark state by a 647-nm excitation laser (MPB Communications) at an intensity of ~2kW cm^2. Dye molecules were concurrently reactivated into the emitting state by a 405-nm excitation laser at a typical power range of 0-1 W cm^{-1} to reach an optimally small fraction of optically resolvable fluorophores in the emitting state. For 3D STORM imaging, the imaging path contained a cylindrical lens to elongate images of single molecules on the proximal and distal sides of the focal plane in opposite directions. ~80,000 frames were collected at 110 frames/second for each image and the raw STORM data were analyzed according to previously described methods (Huang et al., 2008; Rust et al., 2006). Conventional images of Sac6-GFP and Rvs167-2xmScarlet were taken immediately prior to STORM imaging using appropriate laser and filter sets.

Conventional microscopy images of Rvs167-mScarlet were analyzed using Fiji to generate average intensity projections and a median filter was applied and subtracted from the image. Individual late-stage actin patch coordinates were identified using TrackMate (Ershov et al., 2022) and both conventional and superresolved images were cropped at these coordinates using custom Matlab (R2023b) scripts (Ershov et al., 2022; Kaplan et al., 2022). Patches were manually scored for the quality of the actin structure in XY and XZ projections, and the presence of Sac6 and Rvs167 signal, and patches that met the criteria were further analyzed using custom code in Python with Jupyter Notebook. A median filter was applied to each patch and the centroid of phalloidin signal was determined. A radius in X and Y was calculated as the distance between the centroid and the full width half max of the signal from the centroid. The area of the actin patch was calculated as the area of an ellipse: $A = \pi ab$, where a and b are the radii in X and Y. This code is available at the following link:
https://github.com/jennifermhill/Hill_Dissertation/tree/main/STORM_analysis.

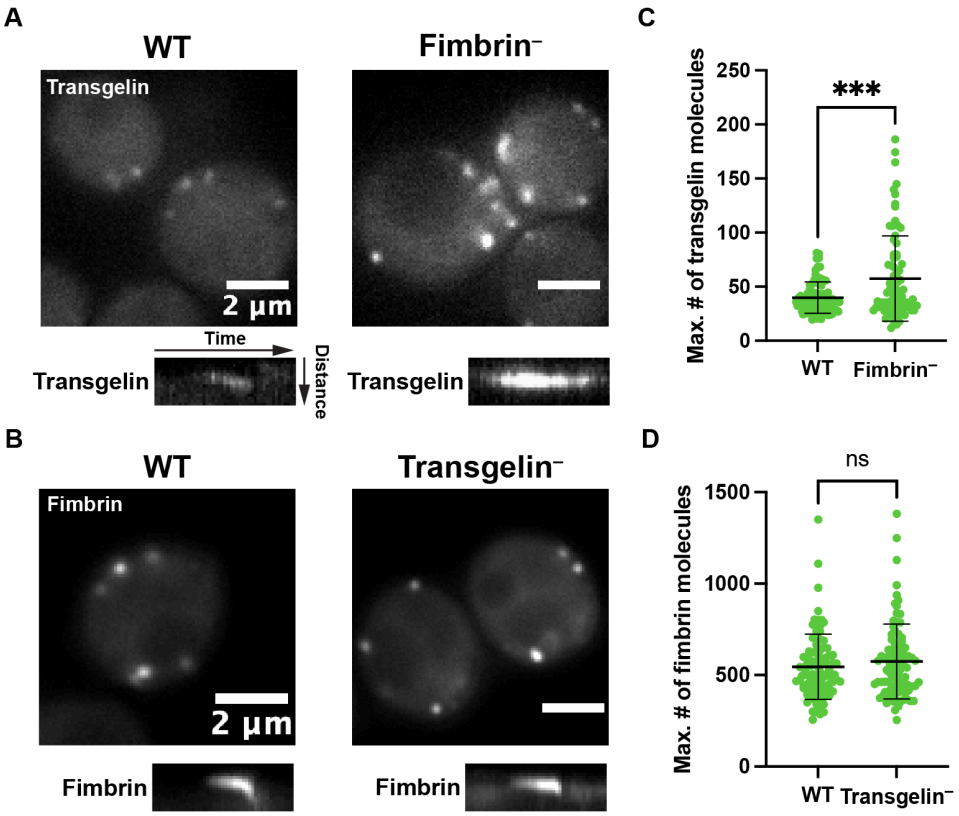

Fig. 2.1. Loss of fimbrin leads to an increase in the number of molecules of transgelin, but loss of transgelin does not affect fimbrin numbers at CME sites. (A), (B). Quantitative microscopy to determine the maximum number of GFP-tagged transgelin (A) or fimbrin (B) molecules at sites of CME in wild-type strains and strains lacking fimbrin (fimbrin⁻) or transgelin (transgelin⁻), respectively. Kymographs of individual sites show a slice from outside the cell (top) to the inside (bottom) over time. (C), (D). Maximum number of molecules of transgelin (C) and fimbrin (D) at CME sites in wild-type and fimbrin⁻ or transgelin⁻ strains, respectively (n=90 sites from ≥10 cells per strain). Error bars show standard deviation.

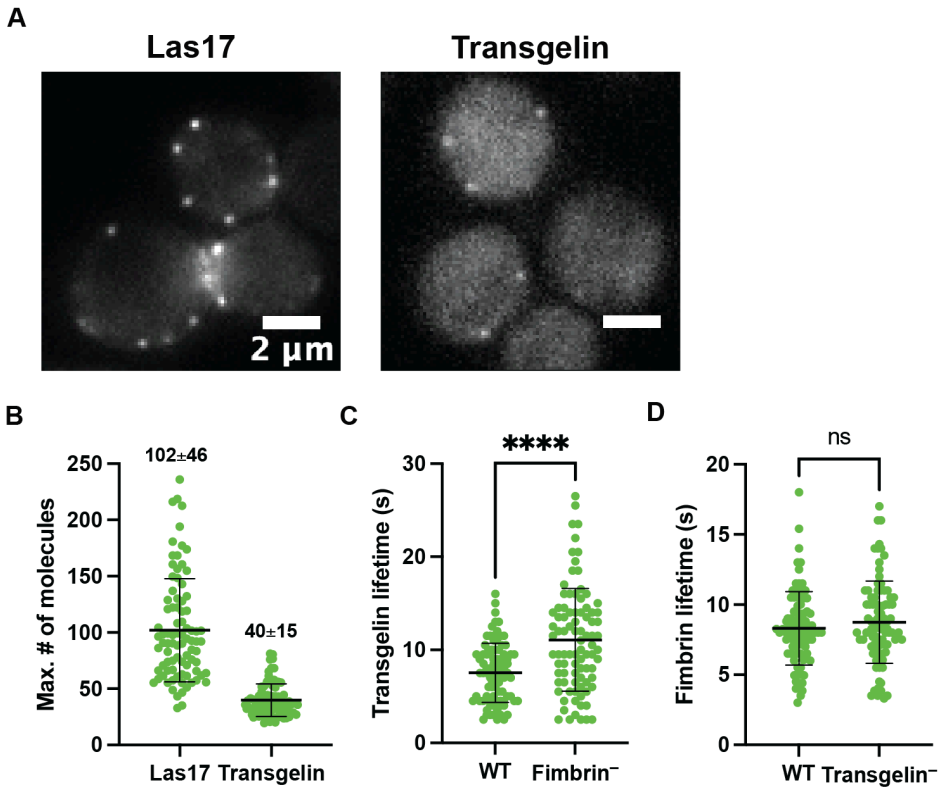

Fig. 2.2. Quantification of maximum number of transgelin molecules arriving at CME sites. (A). Quantitative microscopy of GFP-tagged Las17 (left) and transgelin (right). (B). Quantification of maximum numbers of Las17 molecules and transgelin molecules arriving at CME sites. (C), (D). Lifetimes for transgelin (C) and fimbrin (D) patches at endocytic sites for wild-type and strains lacking fimbrin (fimbrin$^-$) or transgelin (transgelin$^-$), respectively (n=90 sites from ≥10 cells per strain). Error bars show standard deviation.

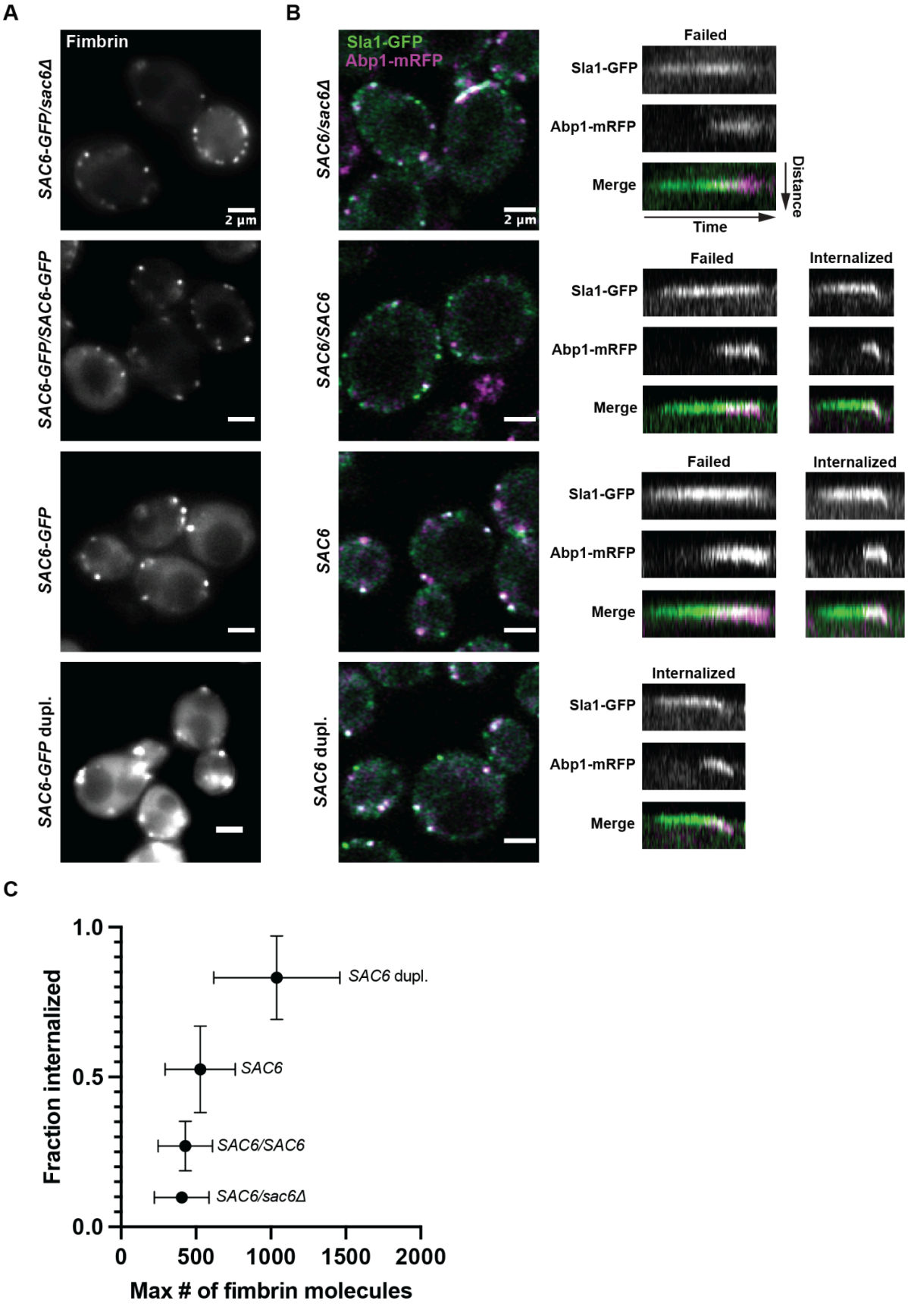
A
Fimbrin
SAC6-GFP/sac6Δ
SAC6-GFP/SAC6-GFP
SAC6-GFP
SAC6-GFP dupl.
2 μm
B
Sla1-GFP
Abp1-mRFP
SAC6/sac6Δ
SAC6/SAC6
SAC6
SAC6 dupl.
Failed
Internalized
Sla1-GFP
Abp1-mRFP
Merge
Distance
Time
C
Fraction internalized
Max # of fimbrin molecules
SAC6 dupl.
SAC6
SAC6/SAC6
SAC6/sac6Δ
0.0
0.5
1.0
0
500
1000
1500
2000

Fig. 2.3. Hypotonic shock hinders CME site internalization depending on crosslinking protein abundance. Cells were grown in media containing 1M sorbitol and shifted to media containing 0.25M sorbitol for five minutes. All strains are in a background containing a deletion of the genes encoding transgelin and Fps1. *SAC6* dupl.: Duplication of the gene encoding fimbrin at the endogenous locus. (A) Quantitative imaging of GFP-tagged fimbrin five minutes after osmotic shock. (B) Imaging of GFP-tagged Sla1 and mRFP-tagged Abp1 five minutes after osmotic shock. Sites where Sla1 and Abp1 hook into the cell were considered internalized. Representative kymographs are shown for all strains. (C) Fraction of endocytic sites that are internalized as a function of the maximum number of fimbrin molecules at endocytic sites five minutes post-shock (n=90 sites from $\geq$10 cells per strain). Error bars show standard deviation.

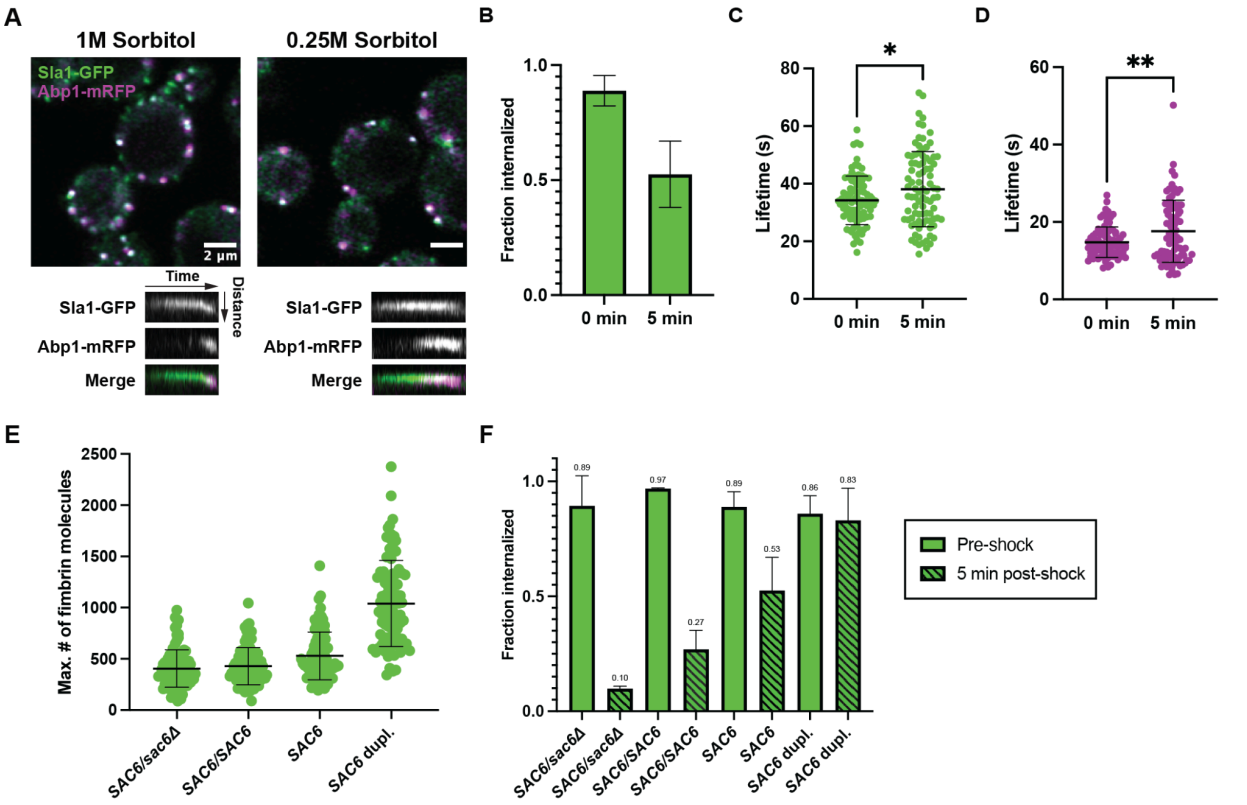

Fig. 2.4. Hypotonic shock stalls endocytosis. Experiment performed as in Fig. 3. (A) WT cells grown in media containing 1M sorbitol (left) or five minutes after shifting to media containing 0.25M sorbitol (right). Representative kymographs are shown for each condition. (B) Fraction of CME sites internalized before and after hypotonic shock. Sites where Sla1 and Abp1 hook into the cell were considered internalized (n=90 sites from ≥10 cells). Error bars show standard deviation. (C), (D) Lifetimes of GFP-tagged Sla1 (C) and mRFP-tagged Abp1 (D) at endocytic sites before and after hypotonic shock (n=90 sites from ≥10 cells). Error bars show standard deviation. (E) Quantification of the maximum number of fimbrin molecules arriving at endocytic sites five minutes after hypotonic shock for strains with different copy numbers of the gene encoding fimbrin (n=90 sites from ≥10 cells). Error bars show standard deviation. (F) Fraction of sites internalized before and after hypotonic shock for strains with different copy numbers of the gene encoding fimbrin (n=3 technical replicates). Error bars show standard deviation.

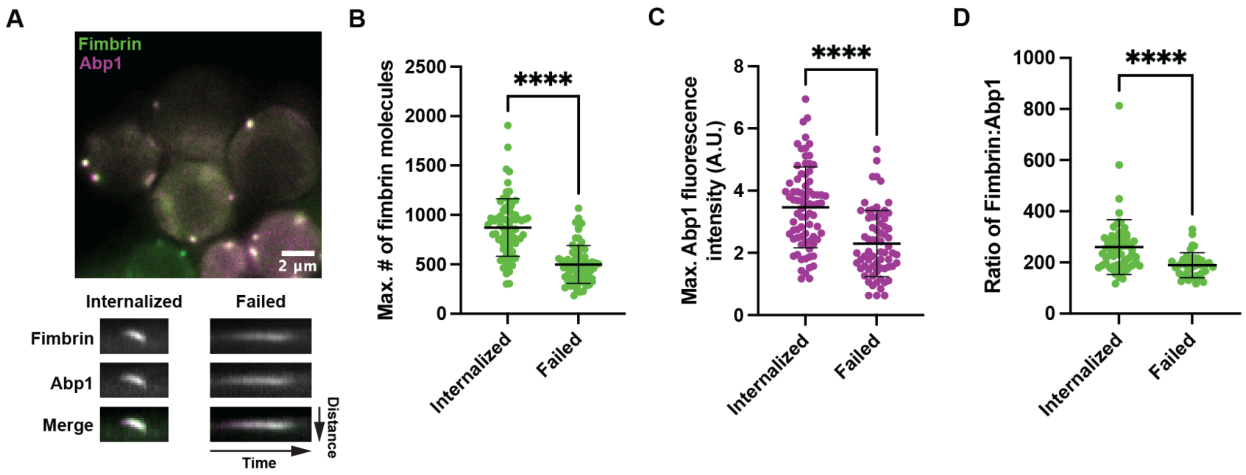

Fig. 2.5. Endocytic sites that internalize under hypotonic shock conditions have a higher maximum number of fimbrin molecules than sites that stall. (A) Cells were grown in 1M sorbitol media and shifted to 0.25M sorbitol media. Fimbrin and Abp1 were imaged after five minutes. (B) Maximum number of fimbrin molecules at endocytic sites that internalize (n=62 sites) or fail (n=38 sites). (C) Maximum fluorescence intensity of mRFP-tagged Abp1 at endocytic sites that internalize (n=62 sites) or fail (n=38 sites). (D) Ratio of the maximum number of fimbrin molecules to Abp1-mRFP fluorescence intensity at endocytic sites that internalize (n=62 sites) or fail (n=38 sites). Error bars show standard deviation.

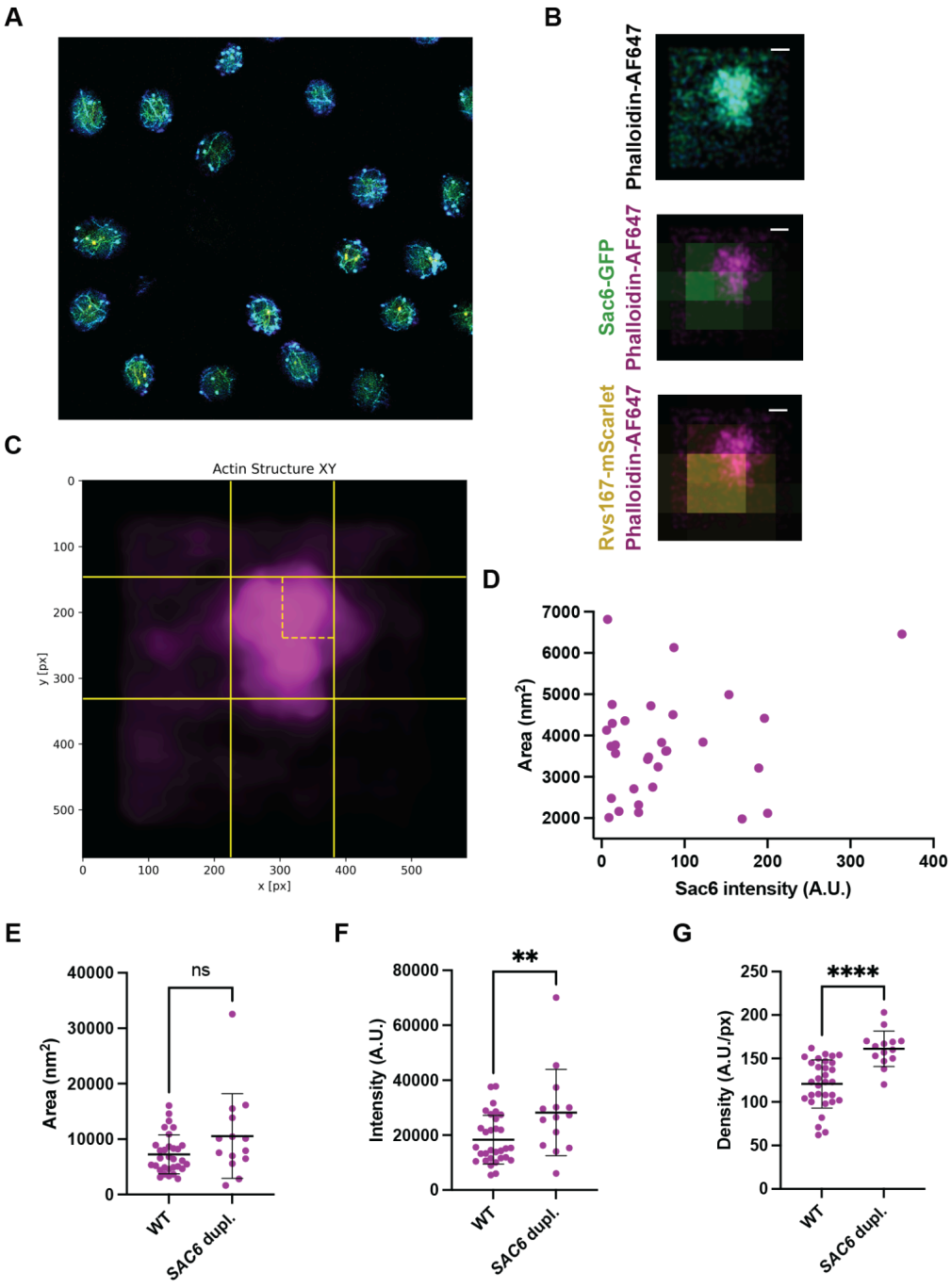

Fig. 2.6. Super-resolution microscopy of phalloidin-labeled actin patches in fixed yeast. (A) STORM image of wild-type fixed yeast stained with phalloidin-AF647. (B) Representative image of a wild-type phalloidin-AF647 stained actin patch (top) with an overlay of Sac6-GFP (middle) and Rvs167-mScarlet (bottom) signal from conventional microscopy. Scale bar = 100 nm. (C) Wild-type phalloidin-AF647 stained actin patch with a median filter applied. Solid lines show the full width at half maximum of signal of the actin patch in X and Y. Dashed lines show the radius of the actin patch in X and Y. (D) Scatter plot of Sac6-GFP intensity from conventional microscopy and corresponding area of the phalloidin-AF647

stained actin patch, approximated as an ellipse, from wild-type cells (n=31). (E) Area, approximated as an ellipse of phalloidin-AF647 stained actin patches from wild-type (n=31) and *SAC6* dupl. cells (n=14). (F) Intensity of phalloidin-AF647 signal of actin patches from wild-type (n=31) and *SAC6* dupl. cells (n=14). (G) Density of phalloidin-AF647 signal of actin patches from wild-type (n=31) and *SAC6* dupl. cells (n=14). Error bars show standard deviation.

Table 2.1. Strains used in this study

Name	Genotype	Source
DCT575	*MATa, his3-Δ200, leu2-3, 112, ura3-52, SCP1-GFP::KanMX*	Drubin Lab
DDY2736	*MATa, his3-Δ200, leu2-3, 112, ura3-52, lys2-801, LAS17-GFP::HIS3,*	Drubin Lab
LCY8.1	*MATα, his3-Δ200, leu2-3,112, ura3-52, SCP1-GFP::HIS3, sac6Δ::cgLEU2*	This study
LCY20.1	*MATα, his3-Δ200, leu2-3,112, ura3-52, lys2-801, scp1Δ::cgURA3, SAC6-GFP::HIS3*	This study
MLY12	*MATα, his3-Δ200, leu2-3,112, ura3-52, SAC6-GFP::HIS3*	Drubin Lab
JHY174.1	*MATα, his3-Δ200, leu2-3,112, ura3-52, scp1Δ::cgURA3, fps1Δ::natNT2, SLA1-GFP::KanMX6, ABP1-mRFP::HIS3*	This study
JHY183.1	*MATα/MATa, his3-Δ200/-, leu2-3,112/-, ura3-52/-, lys2-801/+, scp1Δ::cgURA3/-, fps1Δ::NatNT2/-, SAC6-GFP::HIS3/sac6Δ::cgLEU2*	This study
JHY184.1	*MATα/MATa, his3-Δ200/-, leu2-3,112/-, ura3-52/-, scp1Δ::cgURA3/-, fps1Δ::NatNT2/-, SAC6-GFP::HIS3/SAC6-GFP::HIS3*	This study
JHY182.1	*MATα, his3-Δ200, leu2-3,112, ura3-52, scp1Δ::cgURA3, fps1Δ::NatNT2, SAC6-GFP::HIS3*	This study
JHY218.1	*MATα, his3-Δ200, leu2-3,112, ura3-52, lys2-801, scp1Δ::cgURA3, fps1Δ::NatNT2, SAC6-GFP::HIS3::cgLEU2::SAC6-GFP::HIS3*	This study
JHY178.1	*MATα/MATa, his3-Δ200/-, leu2-3,112/-, ura3-52/-, lys2-801/+, scp1Δ::cgURA3/-, fps1Δ::natNT2/-, SLA1-GFP::KanMX6/+, ABP1-mRFP::HIS3/+, sac6Δ::cgLEU2/+*	This study
JHY179.2	*MATα/MATa, his3-Δ200/-, leu2-3,112/-, ura3-52/-, scp1Δ::cgURA3/-, fps1Δ::natNT2/-, SLA1-GFP::KanMX6/+, ABP1-mRFP::HIS3/+*	This study
JHY176.1	*MATα, his3-Δ200, leu2-3,112, ura3-52, scp1Δ::cgURA3, fps1Δ::natNT2, SAC6::HygMX4::SAC6, SLA1-GFP::KanMX6, ABP1-mRFP::HIS3*	This study
JHY162.1	*MATα, his3-Δ200, leu2-3,112, ura3-52, lys2-801, scp1Δ::cgURA3, fps1Δ::NatNT2, ABP1-mRFP::HIS3, SAC6-GFP::HIS3*	This study
JHY226.1	*MATα, his3-Δ200, leu2-3,112, ura3-52, SAC6-GFP::HIS3, RVS167-2xmScarlet-I::URA3, scp1Δ::KanMX6*	This study

Chapter 3: Actin filament crosslinking proteins organize the actin network to optimize force production in CME

3.1: Introduction

While CME is a highly robust process, actin filament crosslinking is essential for the formation of actin networks capable of carrying out this complex membrane bending process (Kaksonen et al., 2005). Crosslinking proteins participate in most actin-mediated processes, but how actin filament crosslinking affects the geometry and force-generating capabilities of actin networks is still not fully understood. The role of crosslinking proteins in CME has been particularly difficult to study because of the dynamic nature of the process and because CME sites are diffraction-limited, meaning that details of actin filament organization cannot be resolved using conventional or even super-resolution light microscopy techniques. From yeast to humans, the actin filament network at CME sites assembles and disassembles on the time scale of ten to 20 seconds (Kaksonen et al., 2005; Merrifield et al., 2002). Electron microscopy has been used to visualize the geometry of the endocytic actin network in mammalian cells (Collins et al., 2011; Serwas et al., 2022) but lacks information about the dynamics of the process. Given these limitations, mathematical models are highly attractive tools for predicting novel functions of actin crosslinking proteins. When combined with *in vivo* experiments, they can provide deeper mechanistic insights than either technique used alone.

Mathematical models of the actin network and CME have been successfully used to move understanding of the underlying mechanisms of the process forward. A continuous, spatially resolved model of the actin network revealed that assembly of a branched actin network with experimentally constrained viscoelastic properties is sufficient to generate forces on the scale required for internalization of a vesicle in budding yeast (Nickaeen et al., 2019). A model based in physical theory of an elastic surface under force was used to generate predictions about the shape of the membrane invagination as CME progresses (Dmitrieff & Nédélec, 2015). The development of the cytoskeletal simulation engine, Cytosim (Nedelec & Foethke, 2007), has also led to significant progress in agent-based mathematical modeling of the CME. A model of the actin network during CME in mammalian cells revealed the ability of the actin filaments to self-organize to adapt to a range of force requirements (Akamatsu et al., 2020), and a model of budding yeast CME was used to demonstrate the importance of Arp2/3 complex localization at the base of the endocytic pit on a nanoscale level (Mund et al., 2018). Continually expanding on the existing mathematical models of the actin network, in addition to the development of new models at different scales, will prove useful in generating predictions and testing hypotheses of the mechanisms behind force generation in CME.

In this chapter, we investigated the role of actin filament crosslinking proteins in actin filament organization and force generation in budding yeast clathrin-mediated endocytosis. Simulations generated by a mathematical model of the actin filament network during CME in yeast showed that crosslinking proteins promote actin filament network self-organization and concentrate growing filament ends at the plasma membrane, producing higher forces and more efficient internalization. These studies identified novel roles for actin filament crosslinking proteins in force production and actin network organization during budding yeast CME.

3.2: Results and Discussion

3.2.1: Mathematical modeling reveals a force-generating role for actin filament crosslinking proteins

To test the idea that the number of crosslinking proteins recruited to CME sites might be important for endocytic success, we adapted an agent-based mathematical model of the actin network during yeast CME (Mund et al., 2018) to simulate the effects of a range of numbers of crosslinking proteins on vesicle internalization. The model approximates the internalizing vesicle as a cylinder with a hemispherical end attached to a spring that provides a force resistive to internalization (Fig. 3.1A). The magnitude of this force was set based on models of membrane mechanics (Dmitrieff & Nédélec, 2015) such that the actin filament network must overcome an initial force barrier, followed by a linear increase in the force requirement proportional to the distance the vesicle has internalized (Mund et al., 2018). Actin filaments are attached to the tip of the vesicle by a strong actin linker and grow radially outward from this point (Fig. 3.1A). Pre-activated Arp2/3 complex diffuses at the membrane and binds to the growing actin filaments to nucleate daughter filaments at a branching angle of 70° (Fig. 3.1A). Crosslinking proteins diffuse in the cytosolic space and can bind to two actin filaments to form a crosslink (Fig. 3.1A). Both the Arp2/3 complex and crosslinking proteins stochastically bind and unbind actin filaments at rates determined experimentally in *in vitro* studies of the Arp2/3 complex and fimbrin (Mund et al., 2018).

In the absence of crosslinking proteins, actin filaments that grow toward the plasma membrane encounter and bind to the Arp2/3 complex, which nucleates daughter filaments, generating an expanding network of branched actin filaments that generates force to internalize the vesicle throughout a ten-second simulation (Fig. 3.1B, left). We observed that in the presence of crosslinking proteins, crosslinks are formed between actin filaments, and the branched actin filament network internalizes the vesicle further (see white dotted reference line) than in the absence of crosslinking proteins (Fig. 3.1B, right). In all simulations without crosslinking proteins, actin filaments dissociated from the actin network due to Arp2/3 unbinding from the mother filament, while this was never observed in simulations with a pool of 3000 available crosslinking proteins (Fig. 3.1B).

To investigate the effect of the density of crosslinks on the endocytic actin network, we ran simulations with a range of concentrations of crosslinking proteins in the simulation space. The number of crosslinking proteins bound to at least one actin filament in the network after ten seconds increases with the concentration of free crosslinking proteins (Fig. 3.1C and Fig. 3.2A), but the number of crosslinking proteins binding to two actin filaments to form a crosslink (double-bound crosslinkers), plateaus at around 2000 total crosslinking proteins (Fig. 3.1C and Fig. 3.2B). These data suggest that there is an upper limit to the number of double-bound crosslinking proteins that can exist in the branched actin filament network.

We then investigated the effect of the density of double-bound crosslinking proteins on the extent of invagination. To reduce stochastic noise in vesicle internalization, we calculated the 90th percentile of internalization over all simulated time points rather than using the internalized distance at the final time point of the simulation. The extent of invagination increased in proportion to the number of double-bound crosslinkers (Fig. 3.1D and Fig. 3.2C), suggesting that crosslinking of actin filaments within the network enhances force generation during CME internalization. Modeling of membrane mechanics suggests that an energetic snap-through transition occurs when the invagination reaches 60 nm, at which point scission occurs (Hassinger et al., 2017), and the majority of simulations with 1300-1500 double-bound crosslinkers reached this point (Fig. 3.1D). To ensure that this effect is specifically due to the formation of actin filament crosslinks, rather than simply the result of more crosslinking proteins binding in the actin filament network, we also measured the effect of total bound crosslinking proteins in the final network on vesicle internalization. As the total number of bound crosslinking proteins increases to around 2000, internalization of the vesicle also increases, corresponding to the range over which double-bound crosslinkers are increasing in the network (Fig. 3.1E). However, increasing the total number of crosslinking proteins beyond 2000 had little to no effect on the internalization of the invagination, indicating that crosslinking proteins must form filament crosslinks to enhance force generation for internalization.

Interestingly, the effect of crosslinking proteins on internalization is similar across a wide range of force regimes. By increasing the spring constant used to simulate the plasma membrane's resistance to internalization, we modeled the effect of increasing turgor pressure or membrane tension. Networks generated under increased membrane tension conditions still recruit similar numbers of total and double-bound crosslinkers as in simulations with lower membrane tension, plateauing at around 1400-1500 double-bound crosslinkers (Fig. 3.2D and Fig. 3.2E), and these networks do not internalize the membrane as far as those generated with lower membrane tension (Fig. 3.1F). However, at each force regime, internalization still increases with the density of double-bound crosslinkers in the network (Fig. 3.1F and Fig. 3.2F). Taken together, these results suggest that increasing the number of double-bound crosslinkers increases force generation and internalization over a wide range of resistive forces.

3.2.2: Actin filament crosslinking proteins organize the actin network for maximal force production

To investigate how crosslinking proteins contribute to force generation by the actin filament network during CME, we analyzed the organization of actin filaments in simulations with different numbers of crosslinking proteins. Since growing actin filaments can generate forces for internalization, we defined a growing end enrichment score, which represents the enrichment of growing ends in a volume of the actin network at the end of the ten-second simulation. The metric was calculated by subtracting the number of capped actin filament ends in a volume of the network from the number of growing actin filament ends in the same volume. A positive growing end enrichment score indicates a region of the network with more growing than capped actin filament ends. Without crosslinking proteins, the growing end enrichment score is negative for all network regions (Fig. 3.3A, left), indicating that there are no regions of these networks that are enriched for growing ends. However, in simulations starting with 3000 free crosslinkers, equivalent to about 1600 double-bound crosslinkers in the final actin network, the growing end enrichment score is positive in the region of the actin network where filaments contact the membrane (Fig. 3.3A, right), leading to an enrichment of growing filaments ends at the membrane where they can generate force for internalization. This enrichment effect becomes more pronounced throughout the invagination process, such that the final actin network has the highest enrichment of growing ends at the membrane when the membrane is invaginated the most (Fig. 3.4A). Increasing the number of crosslinking proteins also enriches the number of growing ends at the membrane under high membrane tension conditions (Fig. 3.3B). Interestingly, we found that the number of crosslinking proteins has very little effect on the overall axial orientation of actin filaments in the network with respect to the flat membrane, meaning that crosslinking of the actin network does not significantly reorient actin filaments in any direction (Fig. 3.4B and Fig. 3.4C). This result indicates that crosslinking proteins assist in the formation of an actin filament network that is self-organized to generate force through the enrichment of growing filament ends at the plasma membrane.

Growing end enrichment at the plasma membrane in response to elevated numbers of crosslinking proteins suggests that with more crosslinking proteins, the actin filament network has a higher potential energy to be harnessed for force generation. We defined potential polymerization energy as the sum of the polymerization energies of each growing actin filament in contact with the membrane at any given time. Over time, as the network grows and more filaments encounter the membrane, the potential polymerization energy increases (Fig. 3.3C). However, simulations with a larger pool of available crosslinking proteins generate networks that increase their potential polymerization energy at a faster rate than is observed in simulations with fewer crosslinking proteins (Fig. 3.3C). Interestingly, in simulations with small pools of available crosslinking proteins, the potential polymerization energy of the actin filament network plateaus as crosslinking

proteins become saturated in the network (Fig. 3.3C, Fig. 3.4D, and Fig. 3.4E). Additionally, we defined the total polymerization energy of the network as the sum of the potential polymerization energies at each time point. As the free crosslinking protein concentration increases, the total polymerization energy of the network throughout its lifetime increases (Fig. 3.3D), suggesting that crosslinking proteins contribute to the generation of a network with higher potential energy to be harnessed upon actin polymerization.

We also observed the overall compaction of the actin network in simulations with more double-bound crosslinkers, specifically at the contact area between the actin network and the membrane. By quantifying the positions of growing filament ends at the membrane measured radially from the center of the internalizing vesicle in the final second of the simulation, we found that increasing crosslinking proteins decreases the area of contact of filament ends at the membrane such that filament ends are localized closer to the center of the internalizing membrane tubule (Fig. 3.3E). Taken together, these data reveal a role for actin crosslinking proteins in the organization of a compacted actin network enriched in growing filament ends at the membrane, increasing the probability that actin polymerization leads to successful vesicle internalization.

3.2.3: Conclusions

In this study, we set out to determine the effect of actin filament crosslinking proteins on actin network organization and force generation during CME in budding yeast. Our modeling results predict that networks with more crosslinking proteins will internalize more effectively. Simulations with more available crosslinking proteins generate actin networks with increased total and double-bound crosslinking proteins bound in the network, although the number of double-bound crosslinking proteins plateaus at around 1600, suggesting that increasing crosslinking protein availability has a limited effect after this point. Additionally, simulated actin networks with more double-bound crosslinking proteins are capable of internalizing the vesicle more effectively under a wide range of resistive forces, indicating that they assist in force generation by the actin network.

The model also predicts that crosslinking proteins assist in the self-organization of the actin network to optimize the internalization of the plasma membrane driven by actin polymerization, providing a novel role for crosslinking proteins in force generation. Simulated actin networks with more double-bound crosslinking proteins are enriched with growing actin filaments at the membrane, leading to actin networks with a higher potential polymerization energy to be harnessed for internalizing the vesicle. The actin filaments in these networks are also more compact, with their filament ends positioned closer to the center of the internalizing vesicle. Taken together, the data in this chapter reveal a novel role for actin filament crosslinkers in organization of an actin network optimized for force production and internalization of the vesicle during CME.

3.3: Methods

Cytosim model

We modified a previously published Brownian dynamics model of budding yeast CME (Mund et al., 2018) in Cytosim (Nedelec & Foethke, 2007). The simulation is bounded by a cylindrical volume centered around an active patch in which all objects diffuse and, upon collision, may associate stochastically based on programmed parameters determined biochemically. The model consists of actin filaments nucleated by Arp2/3 complexes at the plasma membrane and connected by crosslinking proteins. The 3D actin network is bound to a movable object representing the invagination, and actin filaments produce forces on the membrane to internalize the object against a spring-like resistive force. The resistive force at a given internalized distance is described by the equation: $F(L) = F_0 + k_\pi L$ where F_0 is the initial force barrier to internalize the vesicle, k_π is the spring constant, and L is the distance between the end of the vesicle and the membrane surface. In a modification of the original model, the invagination object was extended to 120 nm, and the rate of Arp2/3 addition remained constant from three to ten seconds of simulation time. To measure the effect of differing numbers of crosslinking proteins, we varied the number of crosslinking proteins available in the cylindrical volume at the start of the simulation from 0 to 6000. To measure the effect of increasing turgor pressure, we varied the spring constant, k_π, on the invagination object from 13,333 pN/nm to 30,000 pN/nm.

Running simulations

Custom scripts in bash were used to run parallel simulations on a high-performance computing server.

Analysis of simulations

Custom code in Python (3.7) with Jupyter Notebook (Project Jupyter) was used to report, read, analyze, and plot the simulations obtained from Cytosim. X, Y = 0 is defined as the center of the pit, and Z = 0 is defined as the membrane. The potential polymerization energy of the network at a given time point was defined as the sum of the potential polymerization energy of all growing actin filaments within a distance of 1.375 nm from the membrane. The potential polymerization energy of an individual actin filament was defined as 9 pN * 2.75 nm * $\sin\theta$ where θ is the angle of incidence with the membrane and $\theta = 0$ is defined as parallel with the membrane. This code is available at the following website: https://github.com/DrubinBarnes/Hill_Cai_Carver_Drubin_2024_Manuscript.

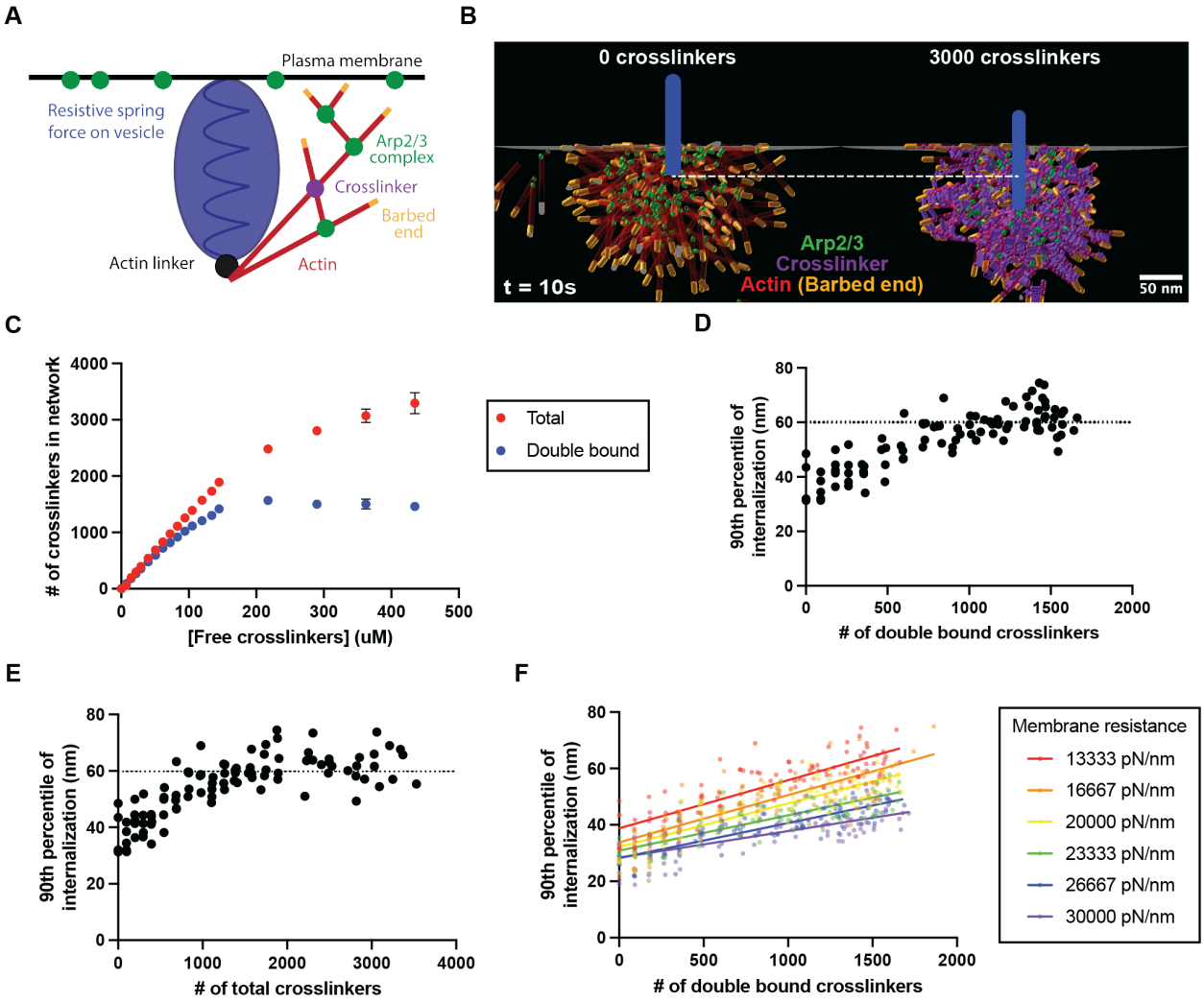

Fig. 3.1. Mathematical modeling reveals that crosslinking proteins contribute to actin network force generation for membrane internalization during CME. (A) Schematic of an agent-based model for the actin network associated with CME sites (Mund et al., 2018). The endocytic vesicle is modeled as a bead on a spring (blue) that resists internalization. Actin filaments attached to the vesicle generate force for internalization by polymerizing at the membrane. (B) Final frame of simulations with pools of either 0 or 3000 available crosslinking proteins. The view shows a slice from the center of the network to reveal the internalized vesicle in the network (blue). (C) Numbers of total and double-bound crosslinkers in the final actin network across a range of free crosslinker concentrations. N=5 simulations, error bars show standard deviation. (D) Scatter plot of the 90th percentile of the extent of vesicle internalization for simulations with a range of numbers of double-bound crosslinkers in the final network. Dotted line at Y=60 nm represents the threshold for snap-through transition and scission. (E) Scatter plot of the 90th percentile of the extent of vesicle internalization for simulations with varying numbers of total crosslinkers in the final network. Dotted line at Y=60 nm represents the threshold for

snap-through transition and scission. (F) Scatter plot of the 90th percentile of the extent of internalization for individual simulations with varying numbers of double-bound crosslinkers and membrane resistances. Solid lines show linear regressions for each set of simulations at a given membrane resistance.

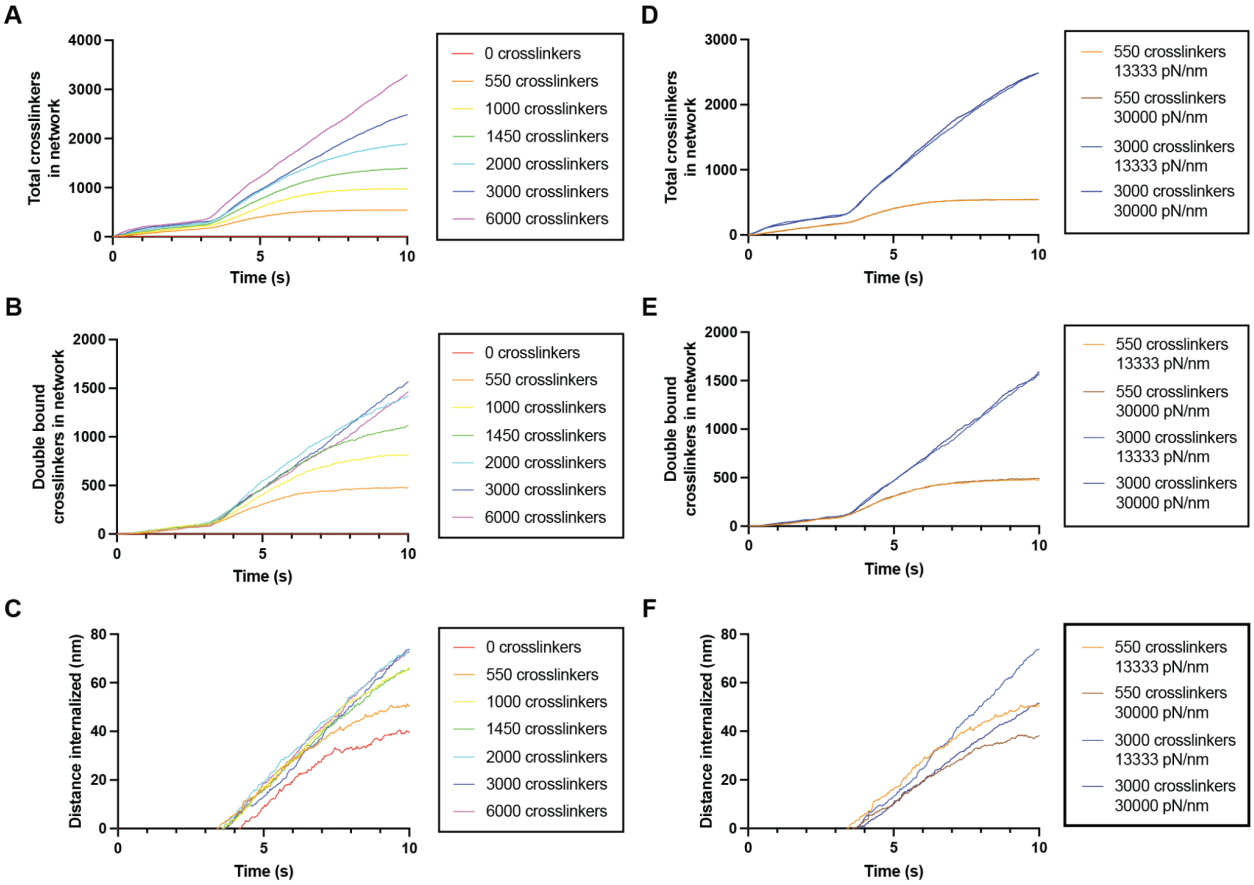

Fig. 3.2. Total and double-bound crosslinkers and vesicle internalization for simulations with various pools of available crosslinking proteins. (A-C) Total number of crosslinking proteins with at least one actin-binding site bound to an actin filament (A), double-bound crosslinkers (B), and distance of vesicle internalization (C) over the duration of simulations with a range of pools of available crosslinking protein numbers with 13333 pN/nm required to internalize the vesicle. N=5 simulations. (D-F) Total number of crosslinking proteins with at least one actin-binding site bound to an actin filament (D), double-bound crosslinkers (E), and distance of vesicle internalization (F) over the duration of simulations with pools of 550 or 3000 available crosslinking proteins and 13333 pN/nm or 30000 pN/nm required to internalize the vesicle. N=5 simulations.

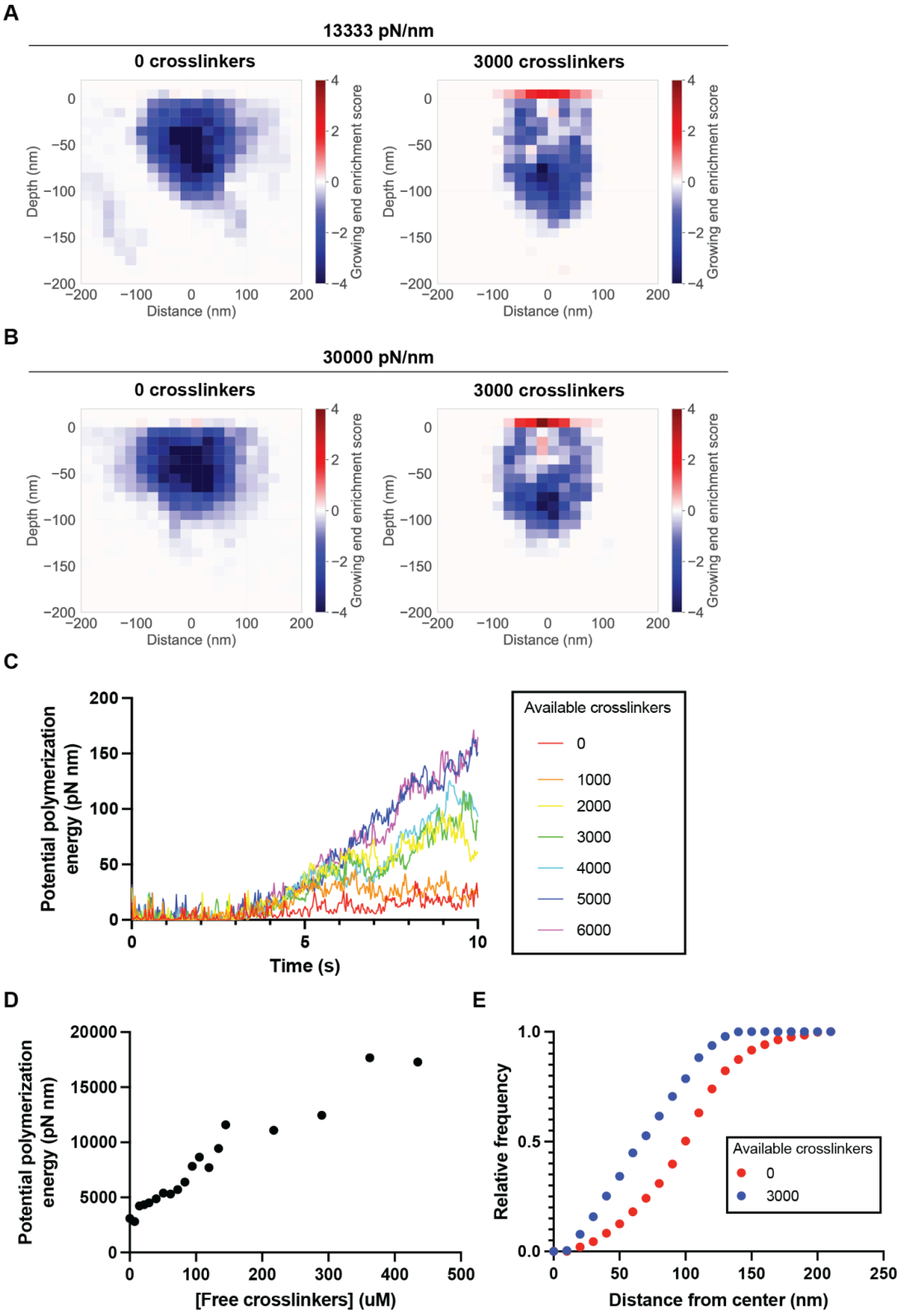

Fig. 3.3. Mathematical modeling predicts self-organization of actin filaments to maximize force production. (A-B) Heat map of enrichment scores for growing ends relative to capped

ends of actin filaments in the final network with pools of either 0 or 3000 available crosslinking proteins and 13333 pN/nm (A) or 30000 pN/nm (B) required to internalize the vesicle. N=5 simulations. (C) Average potential polymerization energy of the actin filament network over the duration of simulations with varying pools of available crosslinking proteins. N=5 simulations. (D) Total potential polymerization energy of the actin filament network as a function of the concentration of free crosslinkers. N=5 simulations. (E) Cumulative distribution functions for the relative frequency of plus ends measured radially from the center of the vesicle for simulations with pools of 0 and 3000 available crosslinking proteins. N=5 simulations.

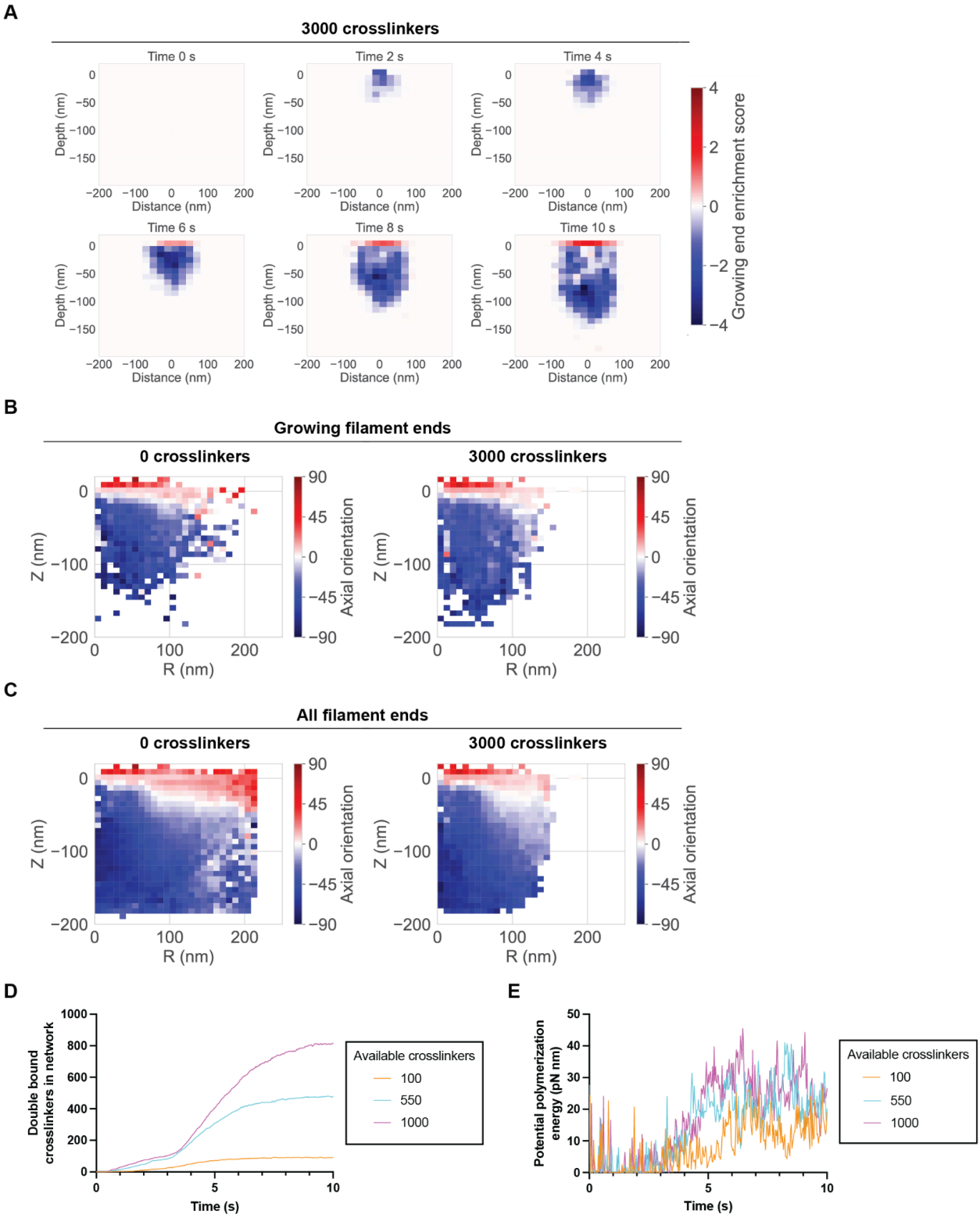

Fig. 3.4. Filament enrichment, axial orientations, and low crosslinking protein simulations. (A) Heat map of enrichment scores for growing actin filament ends relative to capped ends with a pool of 3000 available crosslinking proteins in two-second increments throughout

the length of the simulation. N= 5 simulations. (B) Axial orientation of growing filament ends measured radially from the center of the invagination for simulations with pools of 0 or 3000 available crosslinking proteins. N=5 simulations. (C) Axial orientation of both growing and capped filament ends measured radially from the center of the vesicle for simulations with pools of 0 or 3000 available crosslinking proteins. N=5 simulations. (D) Double-bound crosslinkers over the duration of simulations in the low available crosslinking protein regime. N=5 simulations. (E) Average potential polymerization energy of the actin network over the duration of simulations in the low available crosslinking protein regime. N=5 simulations.

Chapter 4: Myosin-I's motor activity and activation of actin assembly are modular and separable roles

4.1: Introduction

Clathrin-mediated endocytosis in budding yeast occurs under high turgor pressure and therefore requires the forces produced by assembly of a branched actin network and actin-associated proteins (Aghamohammadzadeh & Ayscough, 2009). Myosins are an important contributor to this process both as actin-associated molecular motors and as actin assembly factors (Sun et al., 2006). The myosins involved in CME are the type I myosins, a class of motors in the myosin family (McIntosh & Ostap, 2016). Myosin-I is a small, monomeric, non-processive motor that generally associates with the membrane through a conserved domain in the tail region of the protein (S. V. Kim & Flavell, 2008; McConnell & Tyska, 2010). Myosin-Is are often involved in actin assembly and membrane trafficking processes, and have been implicated in mediation of membrane tension in the cell (McIntosh & Ostap, 2016).

The budding yeast myosin-Is, Myo5 and Myo3, play a critical role as actin-associated proteins in CME. In wild-type cells, the myosin-Is localize to the base of the endocytic invagination where they act as an indispensable connection between actin filaments and the plasma membrane (Pedersen & Drubin, 2019). They are also nucleation promoting factors (NPFs), activating the Arp2/3 complex to generate a branched actin network (Sun et al., 2006). These two myosins are somewhat functionally redundant, although Myo5 is more abundant than Myo3. Cells lacking both myosins build branched actin networks at endocytic sites that are insufficient for internalization of vesicles (Sun et al., 2006). Despite their requirement for CME, their exact mechanism of function is still not fully understood.

Myo5 and Myo3 are long-tailed myosin-Is, harboring several domains in the tail region of the protein that contribute to overall function of the myosin (Lewellyn et al., 2015) (Fig. 4.1A). The tail homology 1 (TH1) domain binds plasma membrane phospholipids and is responsible for recruitment of myosin to endocytic sites, and anchors actin assembly to the membrane. Cells with mutant myosin-Is lacking the TH1 domain build large actin tails at endocytic sites that are incapable of internalizing vesicles (Pedersen & Drubin, 2019). Located C-terminal to the TH1 domain are a Src Homology 3 (SH3) domain and an Arp2/3-binding central acidic (CA) domain, which together with the budding yeast homolog of WIP (WASP interacting protein), Vrp1, recruit and activate the Arp2/3 complex to promote actin filament polymerization at endocytic sites (Geli et al., 2000; Sun et al., 2006). Myosin-I binds Vrp1 through interactions between its SH3 domain and the proline-rich region (PRR) of Vrp1. SH3 or CA domain mutant myosin-Is do not have NPF activity *in vitro*, conferring an endocytic defect *in vivo* (Evangelista et al., 2000; Sun et al., 2006).

Additionally, Myo5 has been shown to be a low-duty-ratio motor with force-insensitive binding and unbinding kinetics *in vitro*, indicating that it is likely to be a power-generating motor, capable of assisting actin assembly in generating force for vesicle internalization (Pedersen et al., 2023). Cells with mutations in the myosin-I motor domain are defective in endocytosis and build actin networks that are largely unable to internalize vesicles (Sun et al., 2006). Given the high modularity of myosin-I in budding yeast and the wide variety of roles played by the individual domains of the protein, there is much to be learned about the interplay between the functional modules of myosin-I in CME.

In this chapter, I investigated whether the functional modules of myosin-I are physically separable or must be present on the same myosin molecule for the success of CME in budding yeast. I generated diploid strains containing combinations of the Myo5 domain mutants, Myo5-motorΔ, Myo5-TH1Δ, and Myo5-SH3Δ, and assessed the ability of these combinations to rescue growth, substrate internalization, and endocytic dynamics. I found that cells containing a copy of the *myo5-TH1Δ* allele were incapable of complementing the other mutants to rescue CME, indicating that the membrane binding TH1 domain must be on the same molecule as motor and NPF activity. In contrast, cells containing a *myo5-motorΔ* allele and a *myo5-SH3Δ* allele were capable of growth, cargo internalization, and endocytic dynamics, indicating that motor activity and NPF activity do not need to be on the same myosin molecule, and suggesting that these functions of myosin-I are modular and fully separable in the context of budding yeast CME.

4.2: Results and Discussion

4.2.1 Myosin-I domain mutant intragenic complementation reveals separable activities

In order to better understand the functional relationships between the myosin-I motor, SH3, and TH1 domains, I asked whether the various activities of each domain need to be on the same myosin molecule in order to achieve regular function of the protein. To address this question, I generated a set of strains to test for intragenic complementation among different combinations of the Myo5 domain mutants: *myo5-TH1Δ/myo5-motorΔ*, *myo5-motorΔ/myo5-SH3Δ*, and *myo5-TH1Δ/myo5-SH3Δ*, in a *myo3*Δ background, since Myo5 and Myo3 are genetically redundant. Additionally, I generated diploid strains containing a combination of each Myo5 domain mutant with the wild-type *MYO5* allele and a *myo5*Δ allele, as positive and negative controls, respectively. I then asked whether each combination of myosin mutants could rescue growth. Growth of the *myo5-TH1Δ/myo5-motorΔ* and *myo5-TH1Δ/myo5-SH3Δ* most closely resembles that of the strains with a *myo5*Δ allele at both 25° and 30°, indicating that these combinations of myosin mutants are not capable of recapitulating wild-type Myo5 function, as it pertains to cell growth (Fig. 4.1B). However, growth of the *myo5-motorΔ/myo5-SH3Δ* strain most closely resembles that of the strains with a wild-type *MYO5* allele at both 25° and 30°,

indicating that the functions still embodied in the Myo5-motorΔ and Myo5-SH3Δ mutants can act in trans (Fig. 4.1B). Thus, myosin-I motor function and NPF activity do not need to be on the same molecule to function inside the cell. On the other hand, motor and NPF activities can only function when paired with membrane binding activity.

In order to determine whether the myosin-I domain mutant combinations can rescue internalization through CME, I quantified internalization of the membrane dye FM4-64. When imaged ten minutes after labeling with the dye, strains with a wild-type *MYO5* allele exhibited staining of internal membrane structures, having internalized ~80% of the dye from the plasma membrane (Fig. 4.2B). In contrast, strains with a *myo5*Δ allele exhibited negligible staining of internal membranes, with only ~35% of the dye internalized from the plasma membrane (Fig. 4.2B), indicating that endocytosis is defective in these strains. The *myo5-TH1Δ/myo5-motorΔ* and *myo5-TH1Δ/myo5-SH3Δ* cells internalized 33.5% and 31.6% of the FM4-64 from the plasma membrane, respectively (Fig. 4.2A and Fig. 4.2B), suggesting that these myosin domain mutants do not complement to rescue FM4-64 internalization and that the membrane binding domain must be on the same molecule as the motor domain and SH3 domain. FM4-64 behavior in the *myo5-motorΔ/myo5-SH3Δ* cells, however, resembled that of strains complemented with a wild-type *MYO5* allele, with 90.5% of the dye internalized from the plasma membrane (Fig. 4.2A and Fig. F4.2B). This result indicates that the *myo5-motorΔ* and *myo5-SH3Δ* alleles functionally complement in the context of substrate internalization, and supports the conclusion that myosin-I motor and NPF activity do not need to be on the same myosin molecule for successful CME.

4.2.2 Myosin-I motor and Arp2/3 complex activation domains can function in *trans* to rescue CME internalization and dynamics

I next investigated CME dynamics in the heterozygous myosin domain mutant strains. To track endocytic internalization, I used a fluorescent fusion of the early coat protein Sla1 as a marker for the endocytic coat, and a fusion of the actin binding protein Abp1 as a marker for the actin network. I then investigated the internalization, organization, and lifetimes of these proteins in the diploid strains. Using Sla1-GFP as a marker for internalization, the fraction of endocytic sites that internalize in strains with a wild-type *MYO5* allele is ~0.95, while the internalized fraction in strains with a *myo5*Δ allele is ~0.1, similar to the internalized fractions in wild-type cells and *myo5*Δ haploid cells, respectively (Lewellyn et al., 2015; Sun et al., 2006) (Fig. 4.3B). The success rate of CME in the *myo5-TH1Δ/myo5-motorΔ* and *myo5-TH1Δ/myo5-SH3Δ* cells is low, similar to that of strains with a *myo5*Δ allele (Fig. 4.3A and Fig. 4.3B), and kymographs of individual endocytic events show that Sla1-GFP and Abp1-mRFP remain at the plasma membrane, indicative of failed CME. However, kymographs of individual endocytic events in *myo5-motorΔ/myo5-SH3Δ* cells show that Sla1-GFP and Abp1-mRFP hook into the cell at the end of the event, with an internalized fraction of 0.87, similar to that of strains with a

wild-type *MYO5* allele (Fig. 4.3A and Fig. 4.3B). Thus, the *myo5-motorΔ* and *myo5-SH3Δ* alleles are capable of complementing to rescue functional endocytic internalization, while neither of the *myo5-TH1Δ* combinations are able to rescue endocytic internalization.

A common phenotype in cells expressing Myo5 lacking a TH1 domain is the formation of actin comets associated with the plasma membrane at endocytic sites, indicative of an actin network incapable of transmitting the force generated by actin polymerization into internalization of the nascent vesicle (Pedersen & Drubin, 2019). In order to test whether the myosin domain mutant combinations displayed this phenotype, I counted the fraction of cells that developed actin comets, read out by Abp1-mRFP structure, throughout a two minute movie. Actin comets were never observed in cells containing a functional *MYO5* allele, and were observed in ~16% of the cells containing only Myo5-TH1Δ (*myo5-TH1Δ/myo5Δ* cells) (Fig. 4.3C), corroborating previous results using haploid cells (Pedersen & Drubin, 2019). In contrast, actin comets were only observed in 0.3% of *myo5-motorΔ/myo5-SH3Δ* cells (Fig. 4.3C). However, for both myosin domain mutant complementations containing a *myo5-TH1Δ*, actin comets were observed at a significantly higher frequency than in strains containing a wild-type *MYO5* allele (Fig. 4.3C), indicating that actin comets are a dominant phenotype caused by Myo5 lacking a TH1 domain.

Lifetimes of endocytic proteins can act as a secondary readout for endocytic success, so I measured the lifetimes of Sla1 and Abp1. In cells containing a wild-type *MYO5* allele, Sla1 and Abp1 lifetimes resembled those in haploid wild-type cells, while in cells containing a *myo5Δ* allele, Sla1 and Abp1 had increased lifetimes, similar to those in haploid *myo5Δ* cells (Kaksonen et al., 2005; Sun et al., 2006) (Fig. 4.3D). Sla1 and Abp1 lifetimes in the *myo5-TH1Δ/myo5-motorΔ* and *myo5-TH1Δ/myo5-SH3Δ*, were also significantly higher, again indicating a defect in endocytosis, and suggesting that these strains are not capable of rescuing endocytic dynamics. The *myo5-motorΔ/myo5-SH3Δ* cells, however, had Sla1 and Abp1 lifetimes that were similar to those in strains containing the wild-type *MYO5* allele (Fig. 4.3D), indicating that Myo5-motorΔ and Myo5-SH3Δ proteins combined are capable of supporting nearly normal endocytic dynamics. Taken together, these data indicate that strains containing a *myo5-TH1Δ* allele are not capable of rescuing endocytic internalization or dynamics, and still generate actin comets at endocytic sites. This result suggests that myosin membrane binding activity must be on the same molecule as motor activity and NPF activity. In contrast, myosin motor and NPF activity do not need to be on the same myosin molecule for successful internalization of the vesicle and wild-type endocytic dynamics.

4.2.3: Conclusions

In this chapter, I have shown that the yeast type I myosin motor and SH3 domain mutants are capable of complementing to rescue growth, membrane internalization, and endocytic dynamics. In a growth assay, colony growth rates match those of strains

containing a wild-type *MYO5* allele, and cells internalize the membrane dye FM4-64 to a similar degree as the *MYO5* containing strains. Additionally, the endocytic coat marker Sla1 and the actin binding protein Abp1 assemble on the plasma membrane and internalize with wild-type dynamics, and endocytic sites in these cells rarely form actin comets seen in strains expressing Myo5 mutants lacking the TH1 domain. This result indicates that functional endocytosis does not require a myosin with motor and NPF activity on the same molecule, and, therefore, that motor activity and Arp2/3 complex activation are functionally separable roles for myosin-I in CME.

In contrast, cells expressing the myosin TH1 mutant with either the motor mutant or the SH3 mutant were not capable of rescuing growth, internalization, or endocytic dynamics. In the growth assay, the growth of these two strains matched the growth of strains containing a *myo5Δ* allele, and cells internalized relatively low amounts of FM4-64. Sla1 and Abp1 remained at the plasma membrane without internalizing, and the lifetimes of these two proteins were significantly higher than in wild-type cells, indicating that CME is inhibited in these strains. This demonstrates that the myosin-I membrane binding domain must be on the same molecule as a functioning motor and SH3 domain for successful endocytosis, indicating that the TH1 domain plays a crucial role in localizing both motor activity and actin polymerization to the plasma membrane. In contrast, myosin-I motor activity and Arp2/3 complex activation can function in *trans* to generate an actin network capable of generating force for internalization.

Endocytic proteins tend to be highly multi-valent. Throughout evolution, the domains are generally conserved, but often appear in different orders or on different proteins in different species (Dergai et al., 2016; Elde et al., 2005; Macro et al., 2012). Considered in combination with the results we presented here, it appears that within the complex network of interacting endocytic proteins, the presence of these domains at the plasma membrane and in the endocytic network is at least in some cases, more important than how those domains are situated in different proteins.

4.3: Methods

Strains and Plasmids

All budding yeast strains were maintained in standard rich media (YPD) at 25°C since *myo5Δ* and domain mutant strains are temperature sensitive. The strains used in this study were derived from the wild-type diploid strain DDY1102 using standard techniques and are listed in Table 4.1. For assaying growth of yeast strains on YPD plates, cells were grown to mid-log phase in liquid standard rich media and serially diluted to OD_{600}=0.1, 0.01, 0.001, and 0.0001. Two μl of each dilution was spotted onto YPD plates, and the plates were incubated at 25° or 30° for 48 hours and photographed.

Live-Cell Imaging

Cells were grown to mid-log phase in imaging media (synthetic minimal media supplemented with adenine, l-histidine, l-leucine, l-lysine, l-methionine, uracil, and 2% glucose) at 25°C and adhered to coverslips coated with 0.2 mg/ml concanavalin A.

For FM4-64 pulse chase experiments, cells were equilibrated with a quick wash of imaging media with 10 μg/ml FM4-64 (Molecular Probes), and then incubated for 5 min at room temperature in imaging media with 10 μg/ml FM4-64. Samples were then washed vigorously with fresh imaging media to remove excess FM4-64. Cells were imaged at room temperature after a 10 min chase on a Nikon Eclipse Ti inverted microscope with a Nikon 100× 1.45-NA Plan Apo λ oil immersion objective using Nikon Elements software. Images were acquired using an Andor IXon X3 EM-CCD camera, and an Andor CSU-X spinning disc confocal setup. FM4-64 was excited using a 488-nm laser and a 500 ms exposure time, and detected with a Chroma 605/52-nm emission filter.

Epifluorescence microscopy of Sla1-GFP and Abp1-mRFP was performed using a Nikon Eclipse Ti inverted microscope with a Nikon 100× 1.4-NA Plan Apo VC oil-immersion objective and an Andor Neo 5.5 sCMOS camera using Nikon Elements software. Coverslips were imaged in an environmental chamber (In Vivo Scientific) pre-warmed and maintained at 25°C. Two color movies of the medial focal plane were acquired sequentially for 2 min using an FF-493/574-Di01 dual-pass dichroic mirror and FF01-512/630-25 dual-pass emission filters (Semrock). GFP and RFP were excited with a Lumencore Spectra X LED light source with 550/515-nm and 470/422-nm excitation filters with 500 ms exposure times for each channel.

Image Analysis

All image analysis was performed using Fiji software (National Institutes of Health). All images and movies were subjected to background subtraction and photobleaching correction (Kaksonen et al., 2003). For FM4-64 pulse-chase experiments, cells that were stained brightly for FM4-64 were removed from analysis as they were considered to be dead or to have compromised plasma membrane permeability. The percent of FM4-64 internalized was calculated by dividing the integrated FM4-64 fluorescence signal inside of the plasma membrane by the integrated FM4-64 fluorescence signal of the entire cell.

For quantification of patch internalization and Sla1-GFP and Abp1-mRFP lifetimes, radial kymographs were generated from cells and chosen at random for quantitative analysis. A patch was judged as “internalized” if it moved at least 200 nm toward the cell interior. A patch was judged as “failed” if it did not move toward the cell interior, moved fewer than 200 nm toward the cell interior, or moved toward the cell interior before returning to its original position.

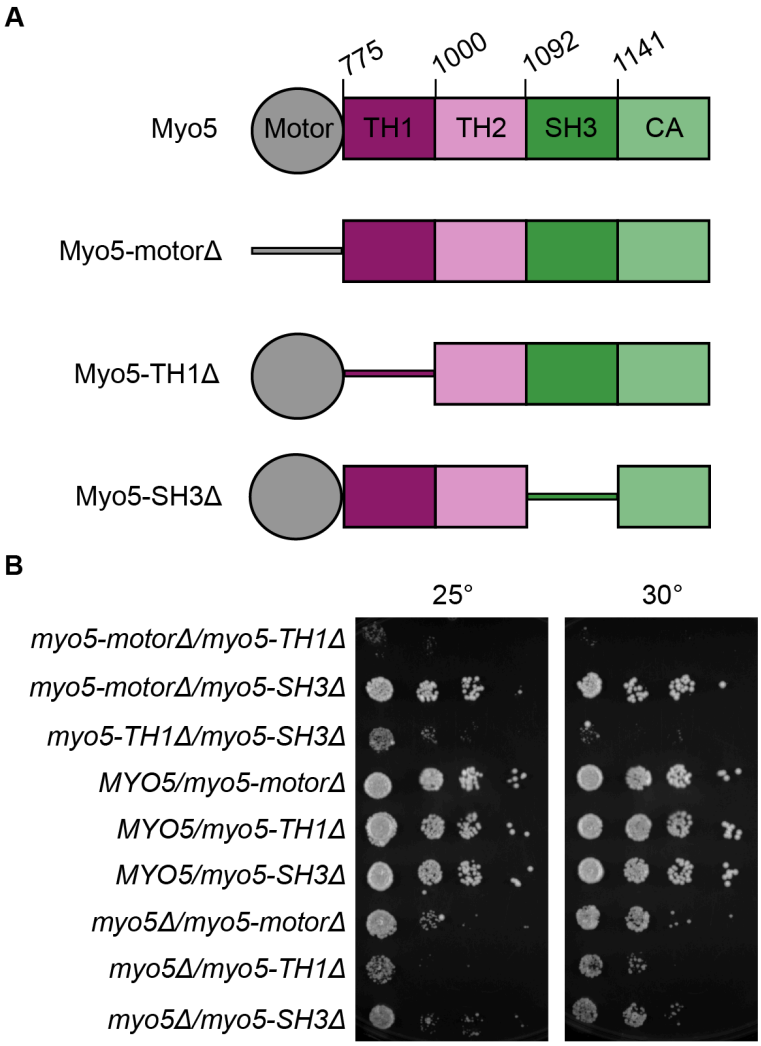

Fig. 4.1. Myosin-I motor and SH3 domain mutants complement to rescue growth in diploid cells. (A) Myosin-I domain structure and mutants. TH1: Tail homology 1, TH2: Tail homology 2, SH3: Src homology 3, CA: Central acidic. (B) Complementation test for diploid strains grown on YPD at 25° and 30° for 48 hours.

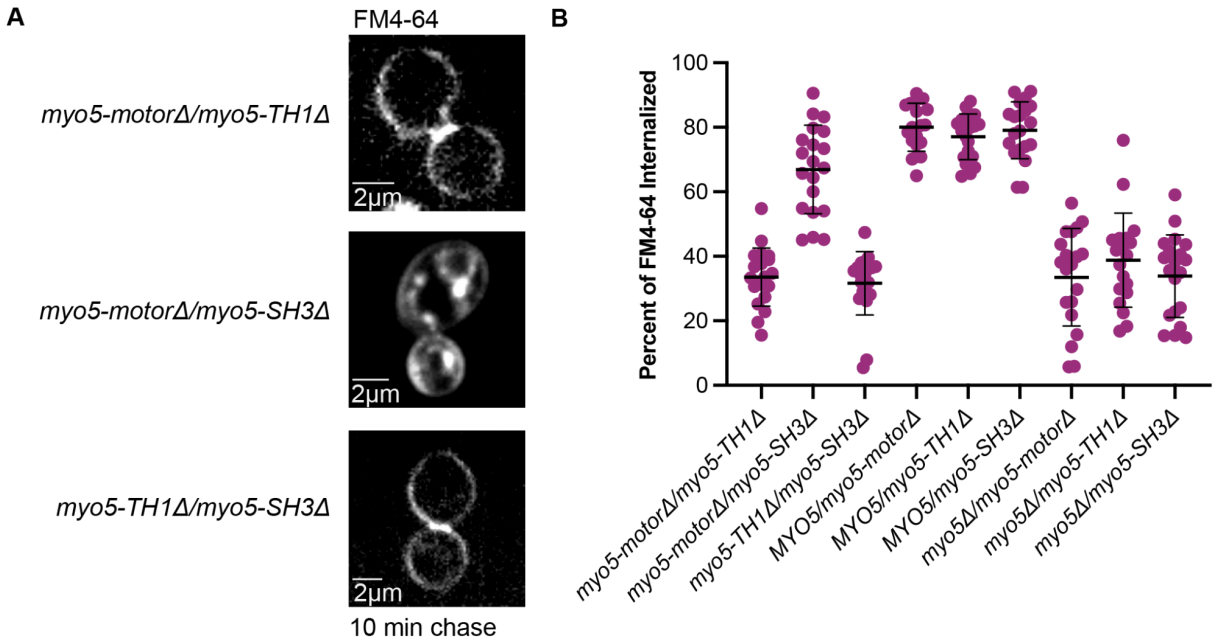

Fig. 4.2. Myosin-I motor and SH3 domain mutants complement to rescue endocytosis of the membrane dye FM4-64. (A) Representative images of FM4-64 signal at the medial plane of cells 10 min post-dye chase. (B) Percent of FM4-64 internalized by myosin-I complementation strains 10 min post-dye chase (n=20 cells). Error bars show standard deviation.

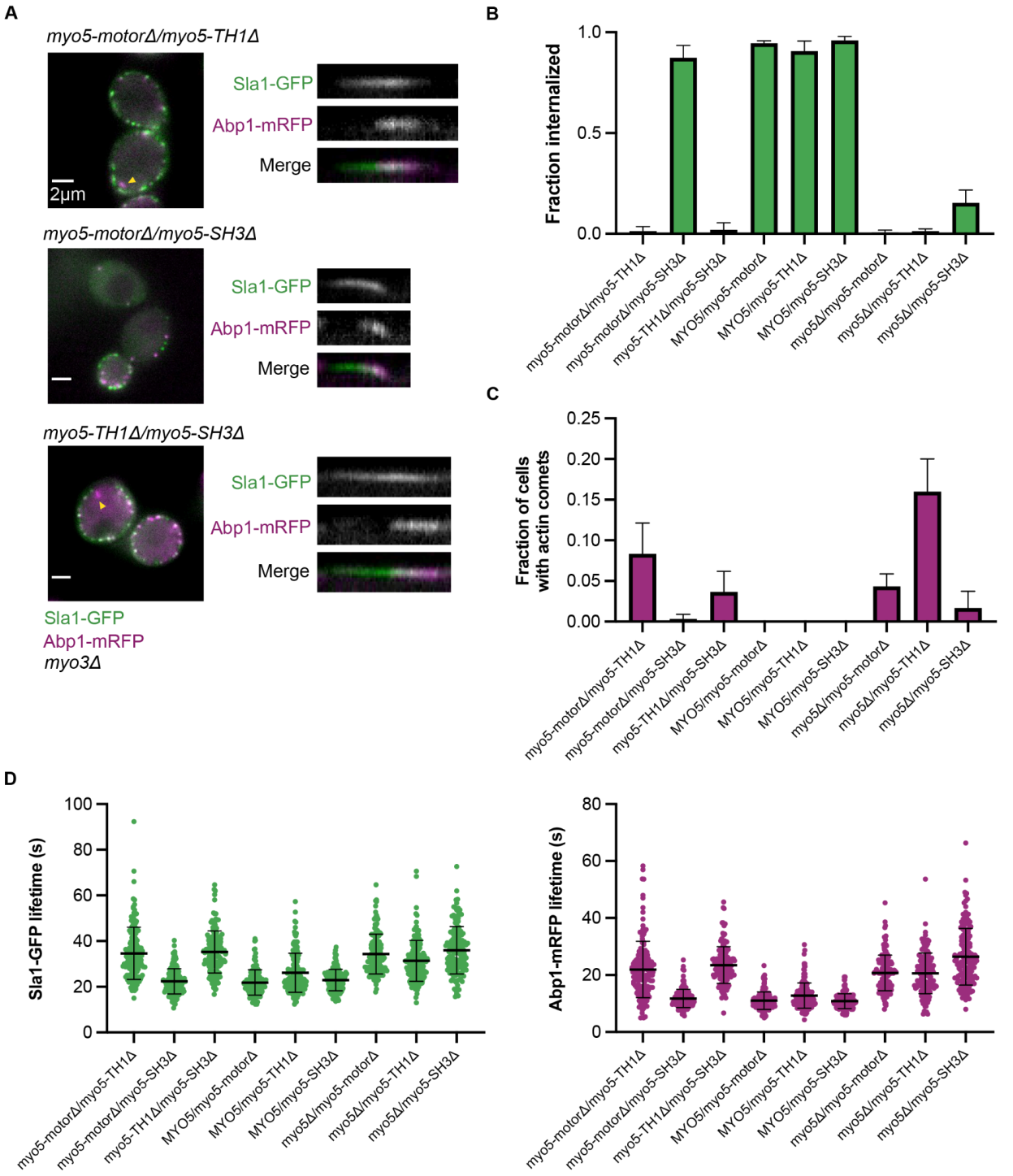

Fig. 4.3. Myosin-I motor and SH3 domain mutants complement to rescue endocytic internalization and dynamics. (A) Representative images of Sla1-GFP and Abp1-mRFP in myosin-I complementation strains and representative kymographs of individual endocytic events in these strains. Yellow arrows indicate endocytic sites with actin comets. (B) Fraction of endocytic sites that internalize in heterozygous myosin-I mutant diploid strains. Sites where Sla1 and Abp1 hook into the cell were considered internalized (n=150 sites

from ≥15 cells). (C) Fraction of cells with actin comets in heterozygous myosin-I mutant diploid strains (n= 150 cells). (D) Sla1-GFP (left) and Abp1-mRFP (right) lifetimes at endocytic sites in myosin-I complementation strains (n=150 sites from ≥15 cells). Error bars show standard deviation.

Table 4.1. Strains used in this study

Name	Genotype	Source
JHY29.1	*MATα/MATa, his3-Δ200/-, leu2-3,112/-, ura3-52/-, lys2-801/+, myo5-TH1Δ-13-myc::URA3/myo5-motorΔ-13Myc::URA3, myo3Δ::cgLEU/-, SLA1-GFP::KanMX/+, ABP1-mRFP::HIS3/+*	This study
JHY30.1	*MATα/MATa, his3-Δ200/-, leu2-3,112/-, ura3-52/-, lys2-801/+, myo5-TH1Δ-13-myc::URA3/myo5-motorΔ-13Myc::URA3, myo3Δ::cgLEU/-, SLA1-GFP::KanMX/+*	This study
JHY31.1	*MATα/MATa, his3-Δ200/-, leu2-3,112/-, ura3-52/-, myo5-motorΔ-13myc::URA3/myo5-SH3Δ-13-myc::URA3, myo3Δ::cgLEU/-, SLA1-GFP::KanMX/+, ABP1-mRFP::HIS3/+*	This study
JHY32.1	*MATα/MATa, his3-Δ200/-, leu2-3,112/-, ura3-52/-, myo5-motorΔ-13myc::URA3/myo5-SH3Δ-13-myc::URA3, myo3Δ::cgLEU/-, SLA1-GFP::KanMX/+*	This study
JHY33.1	*MATα/MATa, his3-Δ200/-, leu2-3,112/-, ura3-52/-, lys2-801/+, myo5-TH1Δ-13-myc::URA3/myo5-SH3Δ-13myc::URA3, myo3Δ::cgLEU/-, SLA1-GFP::KanMX/+, ABP1-mRFP::HIS3/+*	This study
JHY34.1	*MATα/MATa, his3-Δ200/-, leu2-3,112/-, ura3-52/-, lys2-801/+, myo5-TH1Δ-13-myc::URA3/myo5-SH3Δ-13myc::URA3, myo3Δ::cgLEU/-, SLA1-GFP::KanMX/+*	This study
JHY35.1	*MATα/MATa, his3-Δ200/-, leu2-3,112/-, ura3-52/-, myo5-motorΔ-13myc::URA3/MYO5-13-myc::URA3, myo3Δ::cgLEU/-, SLA1-GFP::KanMX/+, ABP1-mRFP::HIS3/+*	This study
JHY36.1	*MATα/MATa, his3-Δ200/-, leu2-3,112/-, ura3-52/-, myo5-motorΔ-13myc::URA3/MYO5-13-myc::URA3, myo3Δ::cgLEU/-, SLA1-GFP::KanMX/+*	This study
JHY37.1	*MATα/MATa, his3-Δ200/-, leu2-3,112/-, ura3-52/-, lys2-801/+, myo5-TH1Δ-13myc::URA3/MYO5-13-myc::URA3, myo3Δ::cgLEU/-, SLA1-GFP::KanMX/+, ABP1-mRFP::HIS3/+*	This study
JHY38.1	*MATα/MATa, his3-Δ200/-, leu2-3,112/-, ura3-52/-, lys2-801/+, myo5-TH1Δ-13myc::URA3/MYO5-13-myc::URA3, myo3Δ::cgLEU/-, SLA1-GFP::KanMX/+*	This study
JHY39.1	*MATα/MATa, his3-Δ200/-, leu2-3,112/-, ura3-52/-, myo5-SH3Δ-13myc::URA3/MYO5-13-myc::URA3, myo3Δ::cgLEU/-, SLA1-GFP::KanMX/+, ABP1-mRFP::HIS3/+*	This study
JHY40.1	*MATα/MATa, his3-Δ200/-, leu2-3,112/-, ura3-52/-, myo5-SH3Δ-13myc::URA3/MYO5-13-myc::URA3, myo3Δ::cgLEU/-, SLA1-GFP::KanMX/+*	This study

JHY41.1	*MATα/MATa, his3-Δ200/-, leu2-3,112/-, ura3-52/-, myo5-motorΔ-13myc::URA3/myo5Δ::URA3, myo3Δ::cgLEU/-, SLA1-GFP::KanMX/+, ABP1-mRFP::HIS3/+*	This study
JHY42.1	*MATα/MATa, his3-Δ200/-, leu2-3,112/-, ura3-52/-, myo5-motorΔ-13myc::URA3/myo5Δ::URA3, myo3Δ::cgLEU/-, SLA1-GFP::KanMX/+*	This study
JHY43.1	*MATα/MATa, his3-Δ200/-, leu2-3,112/-, ura3-52/-, lys2-801/+, myo5-TH1Δ-13myc::URA3/myo5Δ::URA3, myo3Δ::cgLEU/-, SLA1-GFP::KanMX/+, ABP1-mRFP::HIS3/+*	This study
JHY44.1	*MATα/MATa, his3-Δ200/-, leu2-3,112/-, ura3-52/-, lys2-801/+, myo5-TH1Δ-13myc::URA3/myo5Δ::URA3, myo3Δ::cgLEU/-, SLA1-GFP::KanMX/+*	This study
JHY45.1	*MATα/MATa, his3-Δ200/-, leu2-3,112/-, ura3-52/-, myo5-SH3Δ-13myc::URA3/myo5Δ::URA3, myo3Δ::cgLEU/-, SLA1-GFP::KanMX/+, ABP1-mRFP::HIS3/+*	This study
JHY46.1	*MATα/MATa, his3-Δ200/-, leu2-3,112/-, ura3-52/-, myo5-SH3Δ-13myc::URA3/myo5Δ::URA3, myo3Δ::cgLEU/-, SLA1-GFP::KanMX/+*	This study

Chapter 5: Conclusions

In this dissertation, I set out to investigate the mechanisms behind two actin filament-associated proteins, crosslinking proteins and myosins, in assisting in force generation by the actin network during budding yeast CME. Due to the high turgor pressure in budding yeast, internalization of a vesicle from the plasma membrane requires substantial force generated by polymerization of a branched actin network supported by actin-associated proteins such as crosslinking proteins and myosins. Using a combination of live cell microscopy, STORM, and mathematical modeling, I revealed a novel role for actin filament crosslinking proteins in assisting in force generation by the actin filament network during CME under conditions of increased load. I also demonstrated the ability of actin filament crosslinking proteins to organize actin filaments to optimize the transmission of energy from actin filament polymerization into forces that internalize the vesicle. Finally, I showed that motor activity and Arp2/3 complex activation by myosin-I are physically separable protein functions that each must be on the same molecule as a membrane binding module for the success of CME.

Our hypotonic shock experiments indicate that crosslinking proteins are an important force-generating factor for adaptation to high turgor pressure. Hypotonic shock has been used to increase turgor pressure in studies of endocytosis in yeast in multiple previous studies (Abella et al., 2020; Aghamohammadzadeh & Ayscough, 2009; Lemière et al., 2021; Riggi et al., 2019). Deletion of the *FPS1* gene encoding a glycerol transporter leads to a sustained state of increased turgor pressure on the time scale of five to 15 minutes, which causes an endocytic defect (Riggi et al., 2019). In this study, we used hypotonic shock to show that endocytic sites with more crosslinking proteins have a higher likelihood of overcoming the increased energy barrier and internalizing a vesicle, indicating that additional crosslinking proteins generate an actin network capable of generating more force for internalization. A similar example of dosage response in endocytosis has been observed for the type-I myosins, where strains that recruit more myosins to CME sites display increased inward movement speeds during invagination, suggesting that these myosins control the rate of membrane invagination (Manenschijn et al., 2019). Dosage effects of various other components of the CME pathway may provide novel insights into their mechanisms.

We used mathematical modeling of endocytosis to test crosslinking protein importance and mechanism in generating actin networks that generate increased forces for internalization. In the model presented in this study, simulated networks that internalize at least 60 nm and reach the snap-through transition point for internalization have more than 2000 total crosslinking proteins bound in the network. This number is significantly higher than the maximum number of crosslinking proteins measured at sites of CME *in vivo* (~545). Simulated networks that recruit roughly the physiological number of crosslinking proteins fail to internalize to 60 nm (Fig. 3.1E). This result suggests that the model is not

fully capable of recapitulating the forces generated by the actin network *in vivo* and, therefore, is still missing parts required to generate sufficient force for internalization. Myosin-I is a candidate for such a missing part. Additionally, internalization is maximized for networks that accumulate around 1500 double-bound crosslinking proteins and decreases slightly for networks with more than that number, suggesting that there is an optimal number of crosslinking proteins for force generation. Investigation of the nature of actin networks oversaturated with crosslinking proteins both *in silico* and *in vivo* could reveal additional information about their role in CME.

STORM of phalloidin-stained actin patches in fixed yeast revealed that actin patches with more crosslinking proteins are more dense, with more actin per square nanometer, than patches with fewer crosslinking proteins (Fig. 2.6E, Fig 2.6F, and Fig. 2.6G). Additionally, experimental results from hypotonic shock experiments show that CME sites that successfully internalize have both more crosslinking proteins and more actin than sites that fail (Fig. 2.5B and Fig. 2.5C). However, results from simulations of the mathematical model predict that actin networks with more double-bound crosslinking proteins are smaller, with actin filament ends concentrated closer to the vesicle (Fig. 3.3E). Additionally, actin networks from simulations with more double-bound crosslinking proteins have less actin than actin networks in simulations with fewer or no double-bound crosslinkers (data not shown), indicating a discrepancy between the mathematical model and experimental results. It is likely that the current implementation of capping activity and stall force on actin filaments are not sufficient to properly replicate *in vivo* behavior.

A number of relevant recommendations can be made for experimentally constrained adjustments to the mathematical model that would significantly improve its accuracy with respect to the biological system at low computational cost. The current implementation of capping activity in the model automatically caps any actin filament that reaches 60 nm in length, but experimentally constrained, stochastic activity could be added to more closely replicate the lengths of actin filaments when they are capped. Additionally, the budding yeast type-I myosins are required for CME and generate power through motor domain activity (Pedersen et al., 2023; Sun et al., 2006), so including myosins in the model could increase the internalization force generated by the actin network, in tandem with actin polymerization and crosslinking proteins. The data presented in Chapter 3 of this dissertation indicate that myosin-I motor and NPF activity are separable functions, so the two activities could be added to the model separately, allowing us to tease apart the relative individual contributions of each role to the organization and force generation of the actin network during CME.

The model presented in this study also predicts that crosslinking proteins assist in self-organization of actin filaments such that growing filament ends are concentrated at the membrane where they are best situated to generate force for internalization. This type of self-organization of actin networks mediated by interactions between actin-associated proteins and actin filaments has been seen in several other systems. Type-II myosin motor

activity is needed to coalesce randomly oriented actin filaments at formin nodes into a contractile ring during cytokinesis in fission yeast (Coffman et al., 2009; Nakano & Mabuchi, 2006) and nucleation of actin polymerization by ActA from Listeria is sufficient to recruit the necessary downstream actin-binding proteins for assembly of force-producing actin tails (Cameron et al., 1999). The crosslinking protein-directed actin network self-organization observed in this study is maintained even under a high-force regime, suggesting that it may be a critical component of an adaptive response to the varied environmental conditions that budding yeast encounter in the wild. Through the combination of live-cell experiments and mathematical modeling, we uncovered a novel role for actin crosslinking proteins in actin network force generation and organization. Given the high conservation of the proteins involved, we expect that the principles uncovered here will apply broadly to actin networks involved in countless other force-generating processes in a panoply of organisms.

There remains much to be understood about the mechanisms behind force generation by actin filament networks and their associated arrays of protein partners. The results in this dissertation only provide insights into the mechanisms of two actin associated proteins, crosslinking proteins and myosins, but there are a number of other actin filament associated proteins whose roles and mechanisms are still not fully understood. The combination of live cell microscopy to interrogate protein dynamics and STORM and cryo-electron tomography with fixed samples to examine structure and localization on the nanoscale acts as a powerful toolbox for investigating the functions of various actin filament associated proteins. Additionally, future implementation of mathematical modeling across a wide range of scales, from protein structure on the nanoscale, to agent-based mathematical models of actin structures, all the way to population-scale models of cells in tissues will enrich our understanding of the mechanisms behind force generation by actin networks. The feedback between predictions generated by mathematical models and results generated by experimental data can act as an effective engine that will power future discoveries. Uncovering the mechanisms behind force generation by cellular actin filament networks in the future will rely on the innovative use of the full complement of experimental and theoretical techniques at our disposal.

References

Abella, M., Andruck, L., Malengo, G., & Skruzny, M. (2020). Force requirements of endocytic vesicle formation. In *bioRxiv*. bioRxiv. https://doi.org/10.1101/2020.11.11.378273

Aghamohammadzadeh, S., & Ayscough, K. R. (2009). Differential requirements for actin during yeast and mammalian endocytosis. *Nature Cell Biology*, *11*(8), 1039–1042.

Akamatsu, M., Vasan, R., Serwas, D., Ferrin, M. A., Rangamani, P., & Drubin, D. G. (2020). Principles of self-organization and load adaptation by the actin cytoskeleton during clathrin-mediated endocytosis. *eLife*, *9*. https://doi.org/10.7554/eLife.49840

Boettner, D. R., Chi, R. J., & Lemmon, S. K. (2011). Lessons from yeast for clathrin-mediated endocytosis. *Nature Cell Biology*, *14*(1), 2–10.

Bretscher, A., & Weber, K. (1980). Fimbrin, a new microfilament-associated protein present in microvilli and other cell surface structures. *The Journal of Cell Biology*, *86*(1), 335–340.

Cameron, L. A., Footer, M. J., van Oudenaarden, A., & Theriot, J. A. (1999). Motility of ActA protein-coated microspheres driven by actin polymerization. *Proceedings of the National Academy of Sciences of the United States of America*, *96*(9), 4908–4913.

Coffman, V. C., Nile, A. H., Lee, I.-J., Liu, H., & Wu, J.-Q. (2009). Roles of formin nodes and myosin motor activity in Mid1p-dependent contractile-ring assembly during fission yeast cytokinesis. *Molecular Biology of the Cell*, *20*(24), 5195–5210.

Collins, A., Warrington, A., Taylor, K. A., & Svitkina, T. (2011). Structural organization of the actin cytoskeleton at sites of clathrin-mediated endocytosis. *Current Biology: CB*, *21*(14), 1167–1175.

Dergai, M., Iershov, A., Novokhatska, O., Pankivskyi, S., & Rynditch, A. (2016). Evolutionary Changes on the Way to Clathrin-Mediated Endocytosis in Animals. *Genome Biology and Evolution*, *8*(3), 588–606.

Dmitrieff, S., & Nédélec, F. (2015). Membrane Mechanics of Endocytosis in Cells with Turgor. *PLoS Computational Biology*, *11*(10), e1004538.

Elde, N. C., Morgan, G., Winey, M., Sperling, L., & Turkewitz, A. P. (2005). Elucidation of clathrin-mediated endocytosis in tetrahymena reveals an evolutionarily convergent recruitment of dynamin. *PLoS Genetics*, *1*(5), e52.

Ershov, D., Phan, M.-S., Pylvänäinen, J. W., Rigaud, S. U., Le Blanc, L., Charles-Orszag, A., Conway, J. R. W., Laine, R. F., Roy, N. H., Bonazzi, D., Duménil, G., Jacquemet, G., & Tinevez, J.-Y. (2022). TrackMate 7: integrating state-of-the-art segmentation algorithms into tracking pipelines. *Nature Methods*, *19*(7), 829–832.

Evangelista, M., Klebl, B. M., Tong, A. H., Webb, B. A., Leeuw, T., Leberer, E., Whiteway, M., Thomas, D. Y., & Boone, C. (2000). A role for myosin-I in actin assembly through

interactions with Vrp1p, Bee1p, and the Arp2/3 complex. *The Journal of Cell Biology*, *148*(2), 353–362.

Geli, M. I., Lombardi, R., Schmelzl, B., & Riezman, H. (2000). An intact SH3 domain is required for myosin I-induced actin polymerization. *The EMBO Journal*, *19*(16), 4281–4291.

Gheorghe, D. M., Aghamohammadzadeh, S., Smaczynska-de Rooij, I. I., Allwood, E. G., Winder, S. J., & Ayscough, K. R. (2008). Interactions between the yeast SM22 homologue Scp1 and actin demonstrate the importance of actin bundling in endocytosis. *The Journal of Biological Chemistry*, *283*(22), 15037–15046.

Goode, B. L., Eskin, J. A., & Wendland, B. (2015). Actin and endocytosis in budding yeast. *Genetics*, *199*(2), 315–358.

Goodman, A., Goode, B. L., Matsudaira, P., & Fink, G. R. (2003). The Saccharomyces cerevisiae calponin/transgelin homolog Scp1 functions with fimbrin to regulate stability and organization of the actin cytoskeleton. *Molecular Biology of the Cell*, *14*(7), 2617–2629.

Hanein, D., Volkmann, N., Goldsmith, S., Michon, A. M., Lehman, W., Craig, R., DeRosier, D., Almo, S., & Matsudaira, P. (1998). An atomic model of fimbrin binding to F-actin and its implications for filament crosslinking and regulation. *Nature Structural Biology*, *5*(9), 787–792.

Hartman, M. A., & Spudich, J. A. (2012). The myosin superfamily at a glance. *Journal of Cell Science*, *125*(Pt 7), 1627–1632.

Hassinger, J. E., Oster, G., Drubin, D. G., & Rangamani, P. (2017). Design principles for robust vesiculation in clathrin-mediated endocytosis. *Proceedings of the National Academy of Sciences of the United States of America*, *114*(7), E1118–E1127.

Huang, B., Wang, W., Bates, M., & Zhuang, X. (2008). Three-dimensional super-resolution imaging by stochastic optical reconstruction microscopy. *Science*, *319*(5864), 810–813.

Huber, F., Meurer, M., Bunina, D., Kats, I., Maeder, C. I., Stefl, M., Mongis, C., & Knop, M. (2014). PCR Duplication: A One-Step Cloning-Free Method to Generate Duplicated Chromosomal Loci and Interference-Free Expression Reporters in Yeast. *PloS One*, *9*(12), e114590.

Kaksonen, M., Sun, Y., & Drubin, D. G. (2003). A pathway for association of receptors, adaptors, and actin during endocytic internalization. *Cell*, *115*(4), 475–487.

Kaksonen, M., Toret, C. P., & Drubin, D. G. (2005). A modular design for the clathrin- and actin-mediated endocytosis machinery. *Cell*, *123*(2), 305–320.

Kaplan, C., Kenny, S. J., Chen, X., Schöneberg, J., Sitarska, E., Diz-Muñoz, A., Akamatsu, M., Xu, K., & Drubin, D. G. (2022). Load adaptation by endocytic actin networks. *Molecular Biology of the Cell*, *33*(6), ar50.

Kim, K., Yamashita, A., Wear, M. A., Maéda, Y., & Cooper, J. A. (2004). Capping protein binding to actin in yeast: biochemical mechanism and physiological relevance. *The Journal of Cell Biology*, *164*(4), 567–580.

Kim, S. V., & Flavell, R. A. (2008). Myosin I: from yeast to human. *Cellular and Molecular Life Sciences: CMLS*, *65*(14), 2128–2137.

Krey, J. F., & Barr-Gillespie, P. G. (2019). Molecular Composition of Vestibular Hair Bundles. *Cold Spring Harbor Perspectives in Medicine*, *9*(1). https://doi.org/10.1101/cshperspect.a033209

Krey, J. F., Krystofiak, E. S., Dumont, R. A., Vijayakumar, S., Choi, D., Rivero, F., Kachar, B., Jones, S. M., & Barr-Gillespie, P. G. (2016). Plastin 1 widens stereocilia by transforming actin filament packing from hexagonal to liquid. *The Journal of Cell Biology*, *215*(4), 467–482.

Laporte, D., Ojkic, N., Vavylonis, D., & Wu, J.-Q. (2012). α-Actinin and fimbrin cooperate with myosin II to organize actomyosin bundles during contractile-ring assembly. *Molecular Biology of the Cell*, *23*(16), 3094–3110.

Lappalainen, P. (2016). Actin-binding proteins: the long road to understanding the dynamic landscape of cellular actin networks. *Molecular Biology of the Cell*, *27*(16), 2519–2522.

Lemière, J., Ren, Y., & Berro, J. (2021). Rapid adaptation of endocytosis, exocytosis, and eisosomes after an acute increase in membrane tension in yeast cells. *eLife*, *10*. https://doi.org/10.7554/eLife.62084

Lewellyn, E. B., Pedersen, R. T. A., Hong, J., Lu, R., Morrison, H. M., & Drubin, D. G. (2015). An Engineered Minimal WASP-Myosin Fusion Protein Reveals Essential Functions for Endocytosis. *Developmental Cell*, *35*(3), 281–294.

Li, M., Li, S., Lou, Z., Liao, X., Zhao, X., Meng, Z., Bartlam, M., & Rao, Z. (2008). Crystal structure of human transgelin. *Journal of Structural Biology*, *162*(2), 229–236.

Liu, J., Sun, Y., Drubin, D. G., & Oster, G. F. (2009). The mechanochemistry of endocytosis. *PLoS Biology*, *7*(9), e1000204.

Longtine, M. S., McKenzie, A., 3rd, Demarini, D. J., Shah, N. G., Wach, A., Brachat, A., Philippsen, P., & Pringle, J. R. (1998). Additional modules for versatile and economical PCR-based gene deletion and modification in Saccharomyces cerevisiae. *Yeast* , *14*(10), 953–961.

Macro, L., Jaiswal, J. K., & Simon, S. M. (2012). Dynamics of clathrin-mediated endocytosis and its requirement for organelle biogenesis in Dictyostelium. *Journal of Cell Science*, *125*(Pt 23), 5721–5732.

Manenschijn, H. E., Picco, A., Mund, M., Rivier-Cordey, A.-S., Ries, J., & Kaksonen, M. (2019). Type-I myosins promote actin polymerization to drive membrane bending in endocytosis. *eLife*, *8*. https://doi.org/10.7554/eLife.44215

McConnell, R. E., & Tyska, M. J. (2010). Leveraging the membrane - cytoskeleton interface with myosin-1. *Trends in Cell Biology*, *20*(7), 418–426.

McIntosh, B. B., & Ostap, E. M. (2016). Myosin-I molecular motors at a glance. *Journal of Cell Science*, *129*(14), 2689–2695.

Mei, L., Reynolds, M. J., Garbett, D., Gong, R., Meyer, T., & Alushin, G. M. (2022). Structural mechanism for bidirectional actin cross-linking by T-plastin. *Proceedings of the National Academy of Sciences of the United States of America*, *119*(37), e2205370119.

Mellor, H. (2010). The role of formins in filopodia formation. *Biochimica et Biophysica Acta*, *1803*(2), 191–200.

Merrifield, C. J., Feldman, M. E., Wan, L., & Almers, W. (2002). Imaging actin and dynamin recruitment during invagination of single clathrin-coated pits. *Nature Cell Biology*, *4*(9), 691–698.

Mogilner, A., & Rubinstein, B. (2005). The physics of filopodial protrusion. *Biophysical Journal*, *89*(2), 782–795.

Moseley, J. B., & Goode, B. L. (2006). The yeast actin cytoskeleton: from cellular function to biochemical mechanism. *Microbiology and Molecular Biology Reviews: MMBR*, *70*(3), 605–645.

Mund, M., van der Beek, J. A., Deschamps, J., Dmitrieff, S., Hoess, P., Monster, J. L., Picco, A., Nédélec, F., Kaksonen, M., & Ries, J. (2018). Systematic Nanoscale Analysis of Endocytosis Links Efficient Vesicle Formation to Patterned Actin Nucleation. *Cell*, *174*(4), 884–896.e17.

Nakano, K., & Mabuchi, I. (2006). Actin-depolymerizing protein Adf1 is required for formation and maintenance of the contractile ring during cytokinesis in fission yeast. *Molecular Biology of the Cell*, *17*(4), 1933–1945.

Nedelec, F., & Foethke, D. (2007). Collective Langevin dynamics of flexible cytoskeletal fibers. *New Journal of Physics*, *9*(11), 427–427.

Newpher, T. M., Smith, R. P., Lemmon, V., & Lemmon, S. K. (2005). In vivo dynamics of clathrin and its adaptor-dependent recruitment to the actin-based endocytic machinery in yeast. *Developmental Cell*, *9*(1), 87–98.

Nickaeen, M., Berro, J., Pollard, T. D., & Slepchenko, B. M. (2019). Actin assembly produces sufficient forces for endocytosis in yeast. *Molecular Biology of the Cell*, *30*(16), 2014–2024.

Okreglak, V., & Drubin, D. G. (2007). Cofilin recruitment and function during actin-mediated endocytosis dictated by actin nucleotide state. *The Journal of Cell Biology*, *178*(7), 1251–1264.

Ouderkirk, J. L., & Krendel, M. (2014). Myosin 1e is a component of the invadosome core

that contributes to regulation of invadosome dynamics. *Experimental Cell Research*, *322*(2), 265–276.

Pedersen, R. T. A., & Drubin, D. G. (2019). Type I myosins anchor actin assembly to the plasma membrane during clathrin-mediated endocytosis. *The Journal of Cell Biology*, *218*(4), 1138–1147.

Pedersen, R. T. A., Snoberger, A., Pyrpassopoulos, S., Safer, D., Drubin, D. G., & Ostap, E. M. (2023). Endocytic myosin-1 is a force-insensitive, power-generating motor. *The Journal of Cell Biology*, *222*(10). https://doi.org/10.1083/jcb.202303095

Picco, A., & Kaksonen, M. (2017). Precise tracking of the dynamics of multiple proteins in endocytic events. *Methods in Cell Biology*, *139*, 51–68.

Picco, A., Kukulski, W., Manenschijn, H. E., Specht, T., Briggs, J. A. G., & Kaksonen, M. (2018). The contributions of the actin machinery to endocytic membrane bending and vesicle formation. *Molecular Biology of the Cell*, *29*(11), 1346–1358.

Planade, J., Belbahri, R., Boiero Sanders, M., Guillotin, A., du Roure, O., Michelot, A., & Heuvingh, J. (2019). Mechanical stiffness of reconstituted actin patches correlates tightly with endocytosis efficiency. *PLoS Biology*, *17*(10), e3000500.

Pleyer, J., & Fleck, C. (2023). Agent-based models in cellular systems. *Frontiers of Physics*, *10*. https://doi.org/10.3389/fphy.2022.968409

Pollard, T. D. (2016). Actin and Actin-Binding Proteins. *Cold Spring Harbor Perspectives in Biology*, *8*(8). https://doi.org/10.1101/cshperspect.a018226

Pollard, T. D., Blanchoin, L., & Mullins, R. D. (2000). Molecular mechanisms controlling actin filament dynamics in nonmuscle cells. *Annual Review of Biophysics and Biomolecular Structure*, *29*, 545–576.

Rajan, S., Kudryashov, D. S., & Reisler, E. (2023). Actin Bundles Dynamics and Architecture. *Biomolecules*, *13*(3). https://doi.org/10.3390/biom13030450

Reda, B., Alphée, M., Julien, H., & Olivia, du R. (2022). Non-linear elastic properties of actin patches to partially rescue yeast endocytosis efficiency in the absence of the cross-linker Sac6. *Soft Matter*, *18*(7), 1479–1488.

Riggi, M., Bourgoint, C., Macchione, M., Matile, S., Loewith, R., & Roux, A. (2019). TORC2 controls endocytosis through plasma membrane tension. *The Journal of Cell Biology*, *218*(7), 2265–2276.

Riggi, M., Niewola-Staszkowska, K., Chiaruttini, N., Colom, A., Kusmider, B., Mercier, V., Soleimanpour, S., Stahl, M., Matile, S., Roux, A., & Loewith, R. (2018). Decrease in plasma membrane tension triggers PtdIns(4,5)P phase separation to inactivate TORC2. *Nature Cell Biology*, *20*(9), 1043–1051.

Ruppert, C., Godel, J., Müller, R. T., Kroschewski, R., Reinhard, J., & Bähler, M. (1995).

Localization of the rat myosin I molecules myr 1 and myr 2 and in vivo targeting of their tail domains. *Journal of Cell Science*, *108 (Pt 12)*, 3775–3786.

Rust, M. J., Bates, M., & Zhuang, X. (2006). Sub-diffraction-limit imaging by stochastic optical reconstruction microscopy (STORM). *Nature Methods*, *3*(10), 793–795.

Sbalzarini, I. F., & Koumoutsakos, P. (2005). Feature point tracking and trajectory analysis for video imaging in cell biology. *Journal of Structural Biology*, *151*(2), 182–195.

Serwas, D., Akamatsu, M., Moayed, A., Vegesna, K., Vasan, R., Hill, J. M., Schöneberg, J., Davies, K. M., Rangamani, P., & Drubin, D. G. (2022). Mechanistic insights into actin force generation during vesicle formation from cryo-electron tomography. *Developmental Cell*, *57*(9), 1132–1145.e5.

Skau, C. T., Courson, D. S., Bestul, A. J., Winkelman, J. D., Rock, R. S., Sirotkin, V., & Kovar, D. R. (2011). Actin filament bundling by fimbrin is important for endocytosis, cytokinesis, and polarization in fission yeast. *The Journal of Biological Chemistry*, *286*(30), 26964–26977.

Skruzny, M., Brach, T., Ciuffa, R., Rybina, S., Wachsmuth, M., & Kaksonen, M. (2012). Molecular basis for coupling the plasma membrane to the actin cytoskeleton during clathrin-mediated endocytosis. *Proceedings of the National Academy of Sciences of the United States of America*, *109*(38), E2533–E2542.

Stimpson, H. E. M., Toret, C. P., Cheng, A. T., Pauly, B. S., & Drubin, D. G. (2009). Early-arriving Syp1p and Ede1p function in endocytic site placement and formation in budding yeast. *Molecular Biology of the Cell*, *20*(22), 4640–4651.

Sun, Y., Martin, A. C., & Drubin, D. G. (2006). Endocytic internalization in budding yeast requires coordinated actin nucleation and myosin motor activity. *Developmental Cell*, *11*(1), 33–46.

Sun, Y., Schöneberg, J., Chen, X., Jiang, T., Kaplan, C., Xu, K., Pollard, T. D., & Drubin, D. G. (2019). Direct comparison of clathrin-mediated endocytosis in budding and fission yeast reveals conserved and evolvable features. *eLife*, *8*. https://doi.org/10.7554/eLife.50749

Tamás, M. J., Luyten, K., Sutherland, F. C., Hernandez, A., Albertyn, J., Valadi, H., Li, H., Prior, B. A., Kilian, S. G., Ramos, J., Gustafsson, L., Thevelein, J. M., & Hohmann, S. (1999). Fps1p controls the accumulation and release of the compatible solute glycerol in yeast osmoregulation. *Molecular Microbiology*, *31*(4), 1087–1104.

Winder, S. J., Jess, T., & Ayscough, K. R. (2003). SCP1 encodes an actin-bundling protein in yeast. *Biochemical Journal*, *375*(Pt 2), 287–295.

Wojcik, M., Hauser, M., Li, W., Moon, S., & Xu, K. (2015). Graphene-enabled electron microscopy and correlated super-resolution microscopy of wet cells. *Nature Communications*, *6*, 7384.

Wu, X., Wen, B., Lin, L., Shi, W., Li, D., Cheng, Y., Xu, L.-Y., Li, E.-M., & Dong, G. (2021). New insights into the function of Fascin in actin bundling: A combined theoretical and experimental study. *The International Journal of Biochemistry & Cell Biology*, *139*, 106056.